The Journal of Chemical Physics

Deuterium separation at high pressure by nanosecond CO_2 laser multiple-photon dissociation

Cite as: J. Chem. Phys. **72**, 5603 (1980); https://doi.org/10.1063/1.438978

Jack B. Marling, Irving P. Herman and Scott J. Thomas

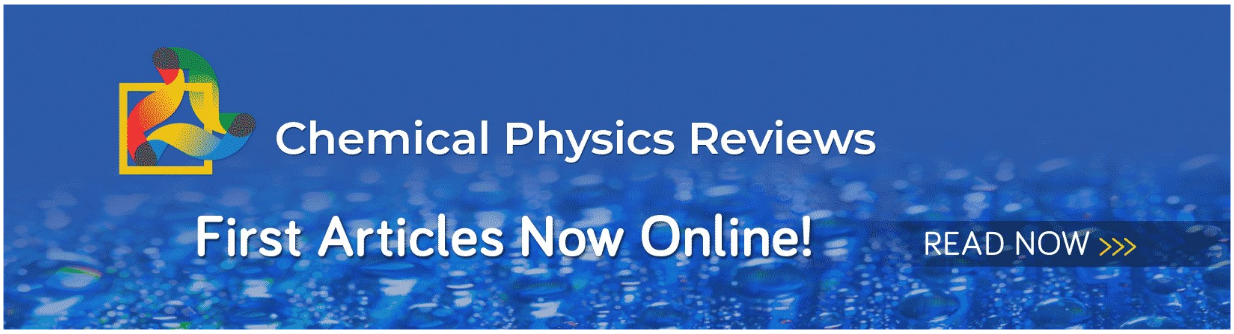

J. Chem. Phys. **72**, 5603 (1980); https://doi.org/10.1063/1.438978

72, 5603

Deuterium separation at high pressure by nanosecond CO_2 laser multiple-photon dissociation

Jack B. Marling and Irving P. Herman

University of California, Lawrence Livermore Laboratory, Livermore, California 94550

Scott J. Thomas

University of California, Los Alamos Scientific Laboratory, Los Alamos, New Mexico 87545

(Received 25 January 1980; accepted 7 February 1980)

Photochemical deuterium separation is evaluated at pressures up to 1 atm using 2 ns duration CO_2 laser pulses to achieve multiple-photon dissociation (MPD) as the isotopic separation step. Photochemical performance is compared for Freon 123 (2,2-dichloro-1,1,1-trifluoroethane), difluoromethane, and trifluoromethane based on deuterium optical selectivity in absorption, photoproduct yield, and single-step deuterium enrichment factor. The absorption coefficient versus energy fluence is measured from 0.01 to 3 J/cm^2 fluence for CF_3CDCl_2, CDF_3, and $CHDF_2$; added buffer gas results in an order-of-magnitude increase in the CDF_3 absorption coefficient. The deuterium optical selectivity in absorption at 0.5 J/cm^2 fluence with added buffer is 80 for CF_3CDCl_2 at 10.65 μ, 800 for $CHDF_2$ at 10.48 μ, and 2500 for CDF_3 at 10.21 μ. The absorption coefficients and hence optical isotopic selectivities are dependent on fluence, and the optical selectivity attains a maximum value of 8000 for CDF_3 below 0.01 J/cm^2 fluence. The deuterium-bearing MPD photoproducts at high pressure are trifluoroethylene for Freon 123, hydrogen fluoride for trifluoromethane, and both hydrogen fluoride and monofluoroacetylene for difluoromethane. Yield data determined by gas chromatography are analyzed using a model describing MPD due to a focused Gaussian beam in an absorbing medium to remove compositional and geometrical effects; this analysis results in a saturation fluence (at which the dissociation probability approaches 100%) of 12 ± 2 J/cm^2 for CF_3CDCl_2, 20 ± 2 J/cm^2 for CDF_3 buffered by 1 atm argon, 30 ± 2 J/cm^2 for CDF_3 buffered by 60–400 Torr CHF_3, and 22 ± 3 J/cm^2 for $CHDF_2$ buffered by 100–400 Torr CH_2F_2. Near unity dissociation probabilities are obtained for samples unbuffered by argon with operating pressures up to 40 Torr for Freon 123, and up to 400 Torr for both difluoromethane and trifluoromethane; the methane derivatives are much more resistant to high pressure collisional quenching than Freon 123. The single-step deuterium enrichment factor is 1200 ± 300 for natural isotopic abundance Freon 123 at 30–100 Torr (10.65 μ) determined by mass spectrometry of the main trifluoroethylene photoproduct. The single-step deuterium enrichment factor determined indirectly from gas chromatographic analysis is 2500 ± 500 for natural difluoromethane at 200 Torr (10.54 μ), and $11{,}000^{+4000}_{-2000}$ for natural trifluoromethane at 100 Torr (10.21 μ). It is concluded that both difluoromethane and trifluoromethane are photochemically satisfactory for viable large-scale laser production of heavy water.

I. INTRODUCTION

Deuterium was the first isotope separated with a laser; this was achieved by ultraviolet photodissociation of formaldehyde D_2CO/H_2CO mixtures in 1972.[1] Natural isotopic abundance deuterium was enriched 15-fold in a single step in 1974,[2] again by formaldehyde photopredissociation; the single-step enrichment of naturally occurring deuterium by this process has been improved to 60-fold using tunable UV ion lasers[3] and more recently to 1650-fold using tunable frequency-doubled dye lasers.[4] Operating pressures were typically 4 Torr in these experiments.[1–4] Because the present cost of deuterium is only about \$3/mol (\$300/kg D_2O), practical separation of deuterium is conceded to pose a very great challenge.[3,5,6] The high electrical efficiency of CO_2 lasers has stimulated efforts in their application to deuterium separation; for example, multiple-photon dissociation (MPD) of natural formaldehyde resulted in 40-fold deuterium enrichment at 40 Torr using high power CO_2 lasers at 10.6 μ in 1976.[7] Recently, 1400-fold single-step deuterium enrichment was obtained in 2,2-dichloro-1,1,1-trifluoroethane (Freon 123) irradiated at 10.65 μ; Freon 123 was selected because of its generally more favorable overall properties for use in a photochemical deuterium separation process.[8] More recently, the highest single-step deuterium enrichment factor has been observed in multiple-photon dissociation of trifluoromethane at 10.2–10.3 μ which has an enrichment factor that exceeds 10 000 in a single step.[9–11]

The rapid development of improved photochemical routes to deuterium separation has encouraged more careful consideration of photochemical reactor design,[12(a)] as well as better overall process analysis.[12(b)] Any potential photochemical deuterium separation process must compete with the already highly developed Girdler-sulfide (GS) process for heavy water production. The GS process utilizes dual temperature chemical exchange between water and hydrogen sulfide and achieves a per stage deuterium separation factor of 1.26.[13] The overall energy costs of the GS process per kg of D_2O are 2.5×10^{10} J of thermal energy and 700 kW h of electrical energy,[13] which are equivalent to 2.6 keV of thermal energy and 0.26 keV of electrical energy per separated D atom. If one assumes that thermal energy can be converted to electrical energy at 33% efficiency, then pho-

---

[a] Work performed under the auspices of the U.S. Department of Energy by Lawrence Livermore Laboratory under contract W-7405-Eng-48.

0021-9606/80/105603-32\$01.00

tochemical routes to deuterium separation (which use primarily electrical energy) may compete with the GS process based on energy considerations if the photochemical process uses less than about 1.13 keV of electrical energy per separated D atom. These simplified considerations are explored further in comparisons of deuterium separation by CO_2 laser multiple-photon dissociation of difluoromethane, trifluoromethane, and Freon 123. These three compounds were selected in a survey of several hundred compounds as the most promising candidate working materials for potentially practical photochemical deuterium separation.[14]

Due to the need to limit photochemical reactor size and gas pumping energy costs, any practical scheme for gas-phase photochemical separation of deuterium must operate at a pressure ≥ 0.1 atm. The high pressure limit for satisfactory yield and enrichment in isotope separation by MPD using the common 100 ns pulse duration TEA CO_2 laser is typically about 1 Torr.[5,9] In MPD studies of "larger" molecules, the dissociation probability is unaffected by a change in laser pulse duration and the accompanying inverse change in laser intensity, when the fluence is held constant.[15(a)] In "smaller" molecules, shortening the pulse width while maintaining constant fluence (and thereby increasing the intensity) actually increases the dissociation probability in many cases.[15(b)] Therefore, if the laser pulse duration is shortened by a factor $f\,(>1)$, the operating partial pressures can be increased by f without changing the number of the detrimental energy-removing collisions that occur during the laser pulse; and additionally, molecules will absorb at least as many quanta after scaling by f in pulse duration as they did before. Therefore, the dissociation probability is not expected to be adversely affected by this scaling procedure unless collisions after the laser pulse successfully siphon energy from molecules (that have been excited to an energy above the dissociation barrier) before the molecules can dissociate. The photochemical MPD properties of the three cited molecules have been investigated at low and high pressures (0–1 atm) using single 2 ns duration pulses from a mode-locked CO_2 laser. Therefore, this study stands as a test (in fact, it is a confirming test) of the scaling properties outlined above.

In Sec. II the employed experimental techniques are presented. The photochemistry of the three molecules under investigation is discussed in Sec. III, based both on observations made in earlier work and in the present studies. The experimental data relating to the absorption cross section, dissociation probability, and the deuterium enrichment factor are presented and analyzed in Sec. IV. Important features of the laser–molecule interaction are discussed in Sec. V A, while in Sec. V B the data are analyzed in relation to practical deuterium separation.

II. EXPERIMENTAL PROCEDURE

A. Laser system

The initial photochemical survey work was performed at low pressure (0.1–3 Torr) using a standard commerical TEA CO_2 laser. The pulse duration was 80 ns FWHM with a tail extending about 500 ns. For the short pulse irradiation experiments at higher pressures, a mode-locked CO_2 laser oscillator followed by a double-pass amplifier was used. This system was designed, constructed, and operated at the Los Alamos Scientific Laboratory, and the experimental layout is detailed in Fig. 1.

The mode-locked pulse from the high-power oscillator was attenuated to give a pulse train of 50 mJ with most of the energy contained in 7–8 pulses. When passed through a GaAs electro-optic switch as shown in Fig. 1, a single 1.6 ns, 10 mJ pulse was obtained. The GaAs electro-optic switch was 8×8×60 mm, having a half-wave voltage of 12.3 kV. A standard laser-triggered spark gap (LTSG) was employed to drive the switch.

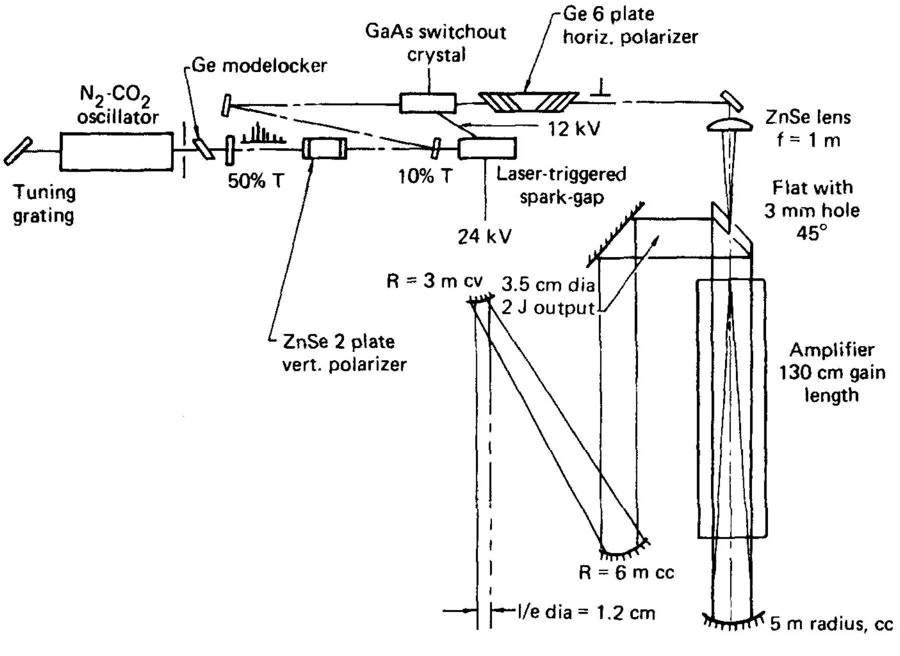

FIG. 1. The mode-locked CO_2 laser system utilizes a grating tuned oscillator with Ge mode locker. The oscillator output triggers a laser-triggered spark gap that opens a 12 ns gate by rotating the polarization 90° using the GaAs switchout crystal. A single mode-locked pulse passes through a six-plate Ge polarizer and undergoes double-pass amplification to 2 J at 10.6 μ in a 2 ns duration pulse.

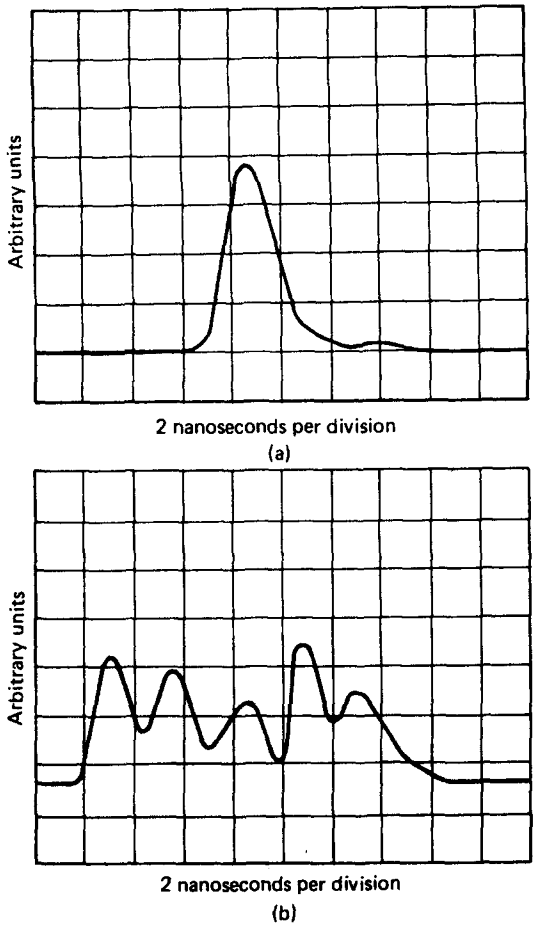

FIG. 2. (a) The upper figure displays a typical mode-locked output pulse of 2 ns full width at half-maximum (FWHM). (b) The lower figure displays a typical 12 ns FWHM duration pulse when the mode locker is turned off. Note the random modes present.

The air supply for the LTSG was filtered and purified with a gas purifier and filter. This improved the reliability of the spark gap. The amplifier was a photopreionized TEA medium having a cross-sectional aperture of 3.5 cm and a 130 cm gain length with a measured gain of 225 (single pass) at $P(20)$, 10.6 μ on discharge center. The main capacitors were charged to 45 kV, while the flash-board capacitors were charged to 35 kV. The capacitor box was filled with oil to discourage corona.

The 10 mJ, 1.6 ns pulse from the switch-out crystal was focused with a 1 m f.l. zinc selenide lens through a 3 mm diameter hole in a 3 in. diameter copper flat. The 3 mm hole was drilled at 45° and positioned below the area intercepted by the output beam. The beam expands from the hole through the gain medium to a 2.5 m f.l. copper mirror which collimates the beam back through the gain medium, and ejects the beam at 90° to the amplifier axis, as shown in Fig. 1. The output energy for the single line operation at $P(20)$, 10.6 μ was 2.0 J, and the output decreased to about 0.5 J on the R-branch lines near 10.2 μ. The pulse repetition rate was one shot per minute. A typical pulse shape is shown in Fig. 2(a); depending on the employed CO_2 laser line, the pulse FWHM varied from about 1.0–2.2 ns. By simply turning off the mode locker, a 12 ns duration pulse was obtained as shown in Fig. 2(b); this pulse duration was determined simply by the 12 ns gate duration of the GaAs switchout crystal. Figure 2(b) shows clearly the characteristic mode beating when mode locking is not present. An 80 ns duration FWHM pulse was obtained when the mode locker was turned off and the switch-out crystal and polarizer shown in Fig. 1 were bypassed. The output beam from the amplifier was recollimated as shown in Fig. 1 to produce a Gaussian beam with 1.2 cm diameter ($1/e^2$ intensity points) and divergence about 1.1 times that of diffraction limited propagation.

The absorption coefficients and the deuterium optical selectivities of the three molecules under investigation were determined by calorimetric measurement of absorbed energy as 2 ns duration CO_2 laser pulses of differing initial energy passed through cells containing known pressures of deuterium-containing or normal gas at room temperature. The experimental layout is indicated in Fig. 3. The 1.2 cm diameter beam was recollimated to a 0.65 cm diameter parallel beam. Calorimeters, placed both before and after the beam entered the 118 cm long absorption cell, sampled the beam to determine the absorbed energy. As shown in Fig. 3, calcium fluoride attenuators of varying thicknesses permitted variation of input energy, and hence permitted a determination of the absorption coefficient α as a function of peak CO_2 laser incident fluence ϕ_{in}. The yield and deuterium enrichment experiments were performed with the laser focused by a 3 m radius of curvature copper mirror into the center of the laser irradiation cells, which were typically 2.5 cm in diameter and 118 cm in length with NaCl end windows at Brewster's angle.

B. Sample preparation

The CF_3CHCl_2 (Freon 123) was used as commerically supplied,[16] and contained approximately 1% Freon 123a impurity ($CF_2ClCHFCl$). This isomer impurity absorbs at 10.0 μ, but is transparent at $P(26)$, 10.65 μ where Freon 123 was irradiated for all experiments. CF_3CDCl_2 at 96%–98% deuterium isotopic purity was prepared by two successive exchanges with D_2O containing 1 mol/l NaOD stirred for an hour at room temperature.[8,17] CH_2F_2 was used as commercially supplied. It contained about 2% CO_2 and less than 0.02% impurities with molecular weight ≤ 100 detectable by gas chromatography (GC) using flame ionization detection. $CHDF_2$ was prepared by fluorination of $CHDBr_2$ using HgF_2.[18] The $CHDBr_2$ was prepared by aqueous exchange between CH_2Br_2 and partially deuterated water under reflux containing 1 mol/l sodium hydroxide catalyst.[19] HgF_2 powder and liquid $CHDBr_2$ were heated in a glass bulb under reflux. Significant SiF_4 was produced using this procedure; however, the SiF_4 was easily removed by exposure to alkaline water. Several trap to trap distillations removed the residual $CHDBr_2$. By this procedure 20% deuterated difluoromethane was prepared containing 64% CH_2F_2, 32% $CHDF_2$, and 4% CD_2F_2. The CHF_3 was used as commercially supplied, and contained less than 0.01% impurities with molecular weight ≤ 100 detectable by GC flame ionization. CDF_3 was used as commercially supplied. It contained about 2% CHF_3 and one sample

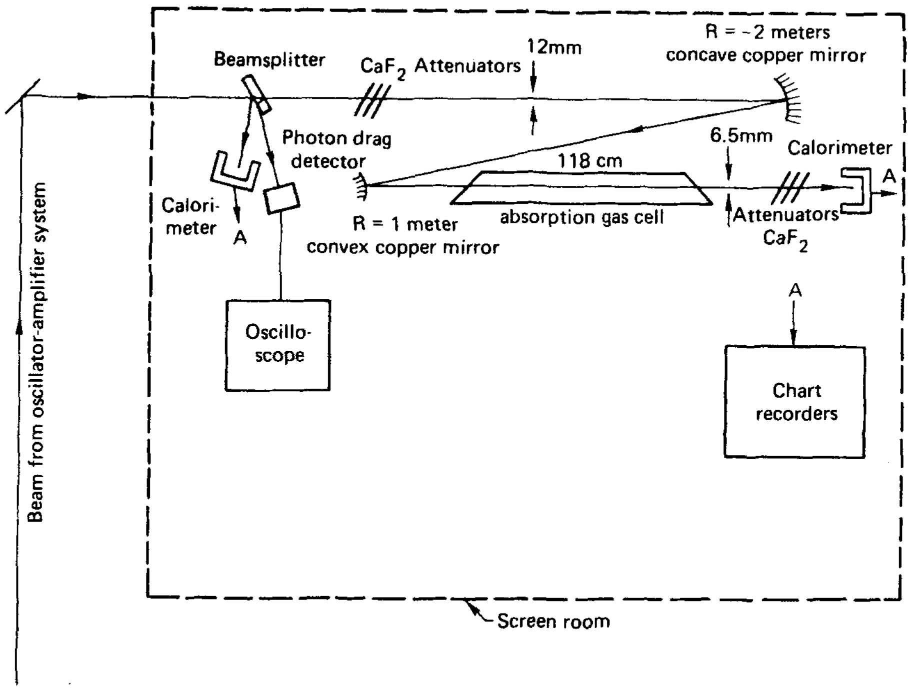

FIG. 3. The experimental layout for energy absorption measurements. A 2 ns pulse enters a screen room, is recollimated to 0.65 cm beam diameter, and is passed through a cell 118 cm in length containing the desired gas. CaF$_2$ attenuators adjust the input and transmitted energy, which is measured by calorimeters and displayed on a dual-axis chart recorder.

(Merck) contained ~ 1% C_2F_4 impurity. A second sample (Stohler Isotope Chemicals) contained < 0.01% C_2F_4 and was also used in this study, to avoid interference with the major CDF_3 decomposition product, also C_2F_4.[9]

The gaseous fill pressure of the absorption and reaction cells was determined by a capacitance manometer below 200 Torr and by a bourdon gauge above 200 Torr, with estimated accuracy of 2%. Isotopic gas mixtures, e.g., $CHF_3 + 2\%\ CDF_3$, were prepared by cryogenically condensing the appropriate gas partial pressures into a separate storage vessel, followed by one cycle of expansion to gas phase and recondensation to insure adequate isotopic mixing. The irradiation cells were then filled by allowing the isotopic mixture to warm from liquid nitrogen temperatures. When the irradiation cells were filled to higher pressure, e.g., 100–1000 Torr total pressure, a different procedure was used. The irradiation cell was first filled with the desired pressure of deuterium-bearing molecule, which was typically 2 Torr when 2 ns duration pulses were used for dissociation. Then the cell was opened just long enough (~ 1 s) to reach equilibrium pressure with the second gas. This procedure was always used for noncondensable secondary gases such as argon. The irradiation cell was then allowed to stand for an hour to allow the gases to mix properly by diffusion.

C. Photoproduct analysis

Photoproduct yield measurements were made by gas chromatography (HP model 5830A) using flame ionization detection. Freon 123 photoproduct yields were analyzed using a 6 foot long, 1/8 in. inside diameter, stainless steel column packed with Chromasorb 102. Trifluoromethane and difluoromethane photoproduct yields were analyzed using a same size stainless steel column packed with Poropak T. Gas samples were withdrawn by syringe extraction from the photolysis cell through a rubber septum port and injected directly into the gas chromatograph. This worked well for experiments above about 20 Torr. Below this pressure the photolyzed sample was first cryogenically condensed into a small volume cell with septum port, yielding about a 90-fold volume compression. Several GC runs in succession on the same sample yielded photoproduct yields in agreement to within a few percent; the reported yields are the average of these runs.

The GC flame ionization detector response was calibrated by mixing equal volumes of gas in a sample cell, and then injecting a sample of this equimolar mixture into the GC for analysis. Calibration was also made by comparison to the response using the thermal conductivity detector, which is relatively insensitive to molecular structure. The relative GC response factors for the various photoproducts are given in Table I. The measured photoproduct yields were divided by the sensitivity factors χ in Table I to normalize results on a per mole (equivalent gas volume) basis.

TABLE I. GC flame ionization detector relative photoproduct sensitivity.

Gas	Sensitivity factor χ
1. Freon 123	1.00
(a) Trifluoroethylene	0.80
(b) Trifluorochloroethylene	0.82
(c) Tetrafluoroethylene	0.98
(d) Trifluorotrichloroethane	1.12
2. Trifluoromethane	1.00
(a) Tetrafluoroethylene	7.94 ± 0.10
3. Difluoromethane	1.00
(a) Monofluoroacetylene	3.5 ± 0.4
(b) Acetylene	6.9 ± 0.7
(c) 1, 1-Difluoroethylene	6.4 ± 1

Isotopic enrichment measurements by mass spectrometry were performed only for Freon 123, since only its major deuterium-bearing photoproduct $CF_2{=}CFD$ is easily analyzed with this technique. An indirect procedure using gas chromatography, first employed by Tuccio and Hartford in analyzing the MPD of trifluoromethane,[11] was used to estimate the high pressure single-step deuterium enrichment factors for trifluoromethane and difluoromethane. This indirect GC method is reasonably accurate as has been shown by Herman and Marling,[10] who used a direct mass-spectrometric procedure for measurement of deuterium enrichment at low pressures (~ 1 Torr) in trifluoromethane. This procedure employed carbon-13 labeling by photolyzing mixtures of $^{12}CDF_3$ and $^{13}CHF_3$, and then analyzing the carbon-13 content of the tetrafluoroethylene photoproduct.[10] Unfortunately, this procedure could not be used at high pressure because of the expense of the $^{13}CHF_3$. Direct mass-spectrometric measurement of the DF/HF photoproduct in trifluoromethane, as well as difluoromethane, photolysis was not attempted in these studies due to the reactivity of hydrogen fluoride. Difluoromethane photolysis also results in monofluoroacetylene $HC{\equiv}CF$ and $DC{\equiv}CF$.[20] However, mass spectrometric analysis involving the parent mass peaks at mass 44 and 45 could not be used because of unavoidable interference by CO_2 impurities. The monofluoroacetylene $\cdot C{\equiv}CD$ and $\cdot C{\equiv}CH$ mass 26 and 25 fragments, respectively, also could not be analyzed due to interference from the small amounts of acetylene produced in difluoromethane photolysis (*vide infra*).[20]

Photolyzed samples of Freon 123 were admitted into the mass spectrometer by first freezing the photoproduct into a cold trap at liquid nitrogen temperature, to allow volatiles to be pumped away. The liquid nitrogen was then replaced by a 2-methylpentane slush at − 153 °C, which allowed adequate vapor pressure for trifluoroethylene (b.p. −56 °C, equilibrium pressure is ~ 30 mTorr at − 153 °C). The Freon 123 vapor pressure (b.p. + 29 °C) was very small at − 153 °C and virtually no interference with the trifluoroethylene mass peaks was observed. The C_2F_2H and C_2F_2D mass fragment peaks at mass 63 and 64, respectively, were used for isotope analysis. The extent of any residual interference from Freon 123 at masses 63 and 64 was uniquely determined from the height of the mass 67 peak ($CHF^{35}Cl$) measured with respect to the mass 63 and 64 peaks in pure unphotolyzed Freon 123 using the same − 153 °C slush bath. Other possible minor photoproducts yielding peaks at mass 63 and 64 that could interfere with analysis, such as difluoroethylene, were not present based on gas chromatographic analysis. A 2.2% contribution at mass 64 due to carbon-13 ($^{13}C\,^{12}CF_2H$ peak) was always subtracted. The single-step deuterium enrichment factor β was then computed from the 64/63 mass ratio divided by the initial deuterium to hydrogen ratio, as described in Eq. (1a):

$$\beta = \frac{\text{D/H final}}{\text{D/H initial}}\ , \tag{1a}$$

$$= \frac{CF_2{=}CFD/CF_2{=}CFH\ \text{(photoproduct)}}{CF_3CDCl_2/CF_3CHCl_2\ \text{(starting material)}}\ . \tag{1b}$$

The initial D/H ratio was determined from the composition of the isotopic mixture prepared by mixing known amounts of CF_3CDCl_2 and CF_3CHCl_2. This initial D/H ratio was typically chosen to be about 0.004. Natural isotopic abundance samples of Freon 123 were also photolyzed; natural Freon 123 is apparently slightly enriched in deuterium, since its natural deuterium content has been measured to be 181 ± 2 ppm.[21] The natural isotopic abundance of deuterium was measured to be 145 ± 5 ppm for trifluoromethane[21]; for difluoromethane the nominal value of 150 ppm was used (equivalent to 300 ppm $CHDF_2$ content).

III. PHOTOCHEMISTRY

A. Freon 123

The photochemistry of Freon 123 has been discussed earlier.[8] The primary observed photoproducts following low pressure photolysis of CF_3CDCl_2 at 10.65 μ in the presence of a large excess of CF_3CHCl_2 are trifluoroethylene, chlorotrifluoroethylene, and 1,1,1-trifluorotrichloroethane, along with a number of minor components; trifluoroethylene is the deuterium-bearing photoproduct. The photoproducts occur by the following main steps[22]:

$$CF_3CDCl_2 + nh\nu(10.65\ \mu) \rightarrow CF_3\dot{C}DCl^{\dagger} + Cl$$

$$(E_{act} \cong 78\ \text{kcal/mol}^{22})\ , \tag{2}$$

$$CF_3\dot{C}DCl^{\dagger} + mh\nu(10.65\ \mu) \rightarrow CF_3\ddot{C}D + Cl\ , \tag{3}$$

$$CF_3\ddot{C}D \rightarrow CF_2{=}CFD\ , \tag{4}$$

$$Cl + CF_3CHCl_2 \rightarrow CF_3\dot{C}Cl_2 + HCl\ , \tag{5}$$

$$Cl + CF_3\dot{C}Cl_2 + M \rightarrow CF_3CCl_3 + M\ , \tag{6}$$

$$CF_3CDCl_2 + n'h\nu(10.65\ \mu)$$

$$\rightarrow CF_3\ddot{C}Cl + DCl\ \ (E_{act} \cong 63.1 \pm 3.8\ \text{kcal/mol}^{22})\ , \tag{7a}$$

$$\longrightarrow CF_2{=}CFCl\ , \tag{7b}$$

where a dagger superscript denotes a vibrationally highly excited molecule. The distribution of products observed in Ref. 8 suggested that Reaction (2) is the main primary step, with Reaction (7) occurring to a much lesser extent. Krajnovich and Lee[23] have arrived at a similar conclusion in a molecular beam investigation of MPD in CF_3CDCl_2. Isotopic scrambling leading to loss of deuterium enrichment (increased production of $CF_2{=}CFH$) may occur by the steps

$$CF_3\dot{C}Cl_2 + CF_3CHCl_2 \rightarrow CF_3CCl_3 + CF_3\dot{C}HCl\ , \tag{8}$$

$$CF_3\dot{C}HCl + M\ (+m'h\nu) \rightarrow CF_2{=}CFH + M + Cl\ , \tag{9}$$

$$CF_3CDCl_2^{\dagger} + CF_3CHCl_2 \rightarrow CF_3CDCl_2 + CF_3CHCl_2^{\dagger}\ , \tag{10}$$

$$CF_3CHCl_2^{\dagger} + mh\nu(10.65\ \mu) + M \rightarrow CF_2{=}CFH + M + 2Cl\ . \tag{11}$$

Steps (8) and (9) suggest possible routes to unwanted production of $CF_2{=}CFH$ via radical reactions. Steps (10) and (11) indicate collisional energy transfer to CF_3CHCl_2 from laser excited CF_3CDCl_2, followed by photodissociation of CF_3CHCl_2. Steps (10) and (11) seem not to be important at high pressure in Freon 123, since essentially no loss in deuterium enrichment is observed at high pressure (see Sec. IV).

B. Trifluoromethane

The photochemistry of trifluoromethane is considerably simpler than that of Freon 123.[9,24] The only observed photoproduct using GC analysis is tetrafluoroethylene; the expected HF/DF product, which is the deuterium-bearing photoproduct, is not detected in our GC apparatus. The important reaction steps are

$$\mathrm{CDF_3} + nh\nu(10.2\text{–}10.3\ \mu) \rightarrow \mathrm{:CF_2 + DF}\ , \tag{12}$$

$$\mathrm{:CF_2 + :CF_2 \rightarrow CF_2{=}CF_2}\ . \tag{13}$$

The thermal activation energy of step (12) is 69.0± 1.6 kcal/mol.[24] The $:CF_2$ radical apparently does *not* react with trifluoromethane; thus, isotopic scrambling according to Reaction (14) apparently does not occur to any detectable extent[10]:

$$\mathrm{:CF_2 + CHF_3 \not\rightarrow CF_2{=}CF_2 + HF}\ . \tag{14}$$

Also, isotopic scrambling by exchange [Eq. (15)] is not important:

$$\mathrm{DF + CHF_3 \not\rightarrow HF + CDF_3}\ . \tag{15}$$

This was verified by failure to detect CDF_3 when an equal molar mixture of DF and CHF_3 gases at 20 Torr was allowed to stand together at 220 °C for one week.[10]

C. Difluoromethane

The MPD photochemistry of difluoromethane is slightly more complex than for trifluoromethane; it is discussed here for the first time based on the findings in this study. In analogy to trifluoromethane photochemistry, the primary step is also elimination of HF [Eq. (16)] with a thermal activation energy of 70.2± 1.8 kcal/mol.[24] The presence of two hydrogen sites on difluoromethane may allow for some isotopic fractionation due to the kinetic isotope effect. The major reaction steps may be written as

$$\mathrm{CHDF_2} + nh\nu(10.5\ \mu) \rightarrow \mathrm{:CDF + HF}\ , \tag{16a}$$

$$\rightarrow \mathrm{:CHF + DF}\ , \tag{16b}$$

$$\mathrm{:CHF + :CDF \rightarrow CHF{=}CDF^{\dagger} \rightarrow HC{\equiv}CF + DF}\ , \tag{17a}$$

$$\rightarrow \mathrm{DC{\equiv}CF + HF}\ . \tag{17b}$$

Since HF elimination is expected to be favored over DF elimination in both Reactions (16) and (17), additional deuterium concentration should occur in the monofluoroacetylene product in Eq. (17). Both $DC{\equiv}CF$ and DF are deuterium-bearing products in this kinetic scheme.

In this study monofluoroacetylene is by far the major observed (GC-detected) dissociation product, while the 1,2-difluoroethylene yield is observed to be less than 1% of the monofluoroacetylene peak. The $CHF{=}CDF^{\dagger}$ produced by Reaction (17a) has at least 110 kcal/mol of internal energy, based on a free energy of about +20 kcal/mol for the :CHF radical.[25] Since this is much greater than the typical barrier height for HF elimination from ethylenes of ≃ 70 kcal/mol,[24,26,27] essentially all :CHF recombination leads to rapid formation of $HC{\equiv}CF+HF$, as is observed here.

The :CHF radicals produced by the primary dissociation step (16) may also attack the parent CH_2F_2 molecule in step (18) to produce a transient highly excited $C_2H_3F_3^{\dagger}$ molecule[24]; this would then dissociate, resulting in production of internally excited 1,1-difluoroethylene, according to Reaction (19):

$$\mathrm{:CHF + CH_2F_2 \rightarrow C_2H_3F_3^{\dagger}}\ , \tag{18}$$

$$\mathrm{C_2H_3F_3^{\dagger} \rightarrow CF_2{=}CH_2^{\dagger} + HF}\ , \tag{19}$$

$$\mathrm{CF_2{=}CH_2^{\dagger} \rightarrow FC{\equiv}CH + HF}\ . \tag{20}$$

This mechanism could also conceivably produce $HC{\equiv}CF$ via step (20). However, this does not occur for the following reasons: $C_2H_3F_3^{\dagger}$ has an internal energy of at least 73 ±10 kcal/mol, which is close to the measured HF elimination barrier of ~ 70 kcal/mol in this molecule[27]; thus, Reaction (19) is likely to occur. Reactions (18) and (19) have also been hypothesized as the main steps in the thermal decomposition of CH_2F_2,[24] in which $CF_2{=}CH_2$ was actually observed as the dominant product. A minimum total of 49 kcal/mol is available to $CF_2{=}CH_2$ and HF in Eq. (19); because of the limited energy available to $C_2H_3F_3^{\dagger}$, not much more than ~ 50 kcal/mol can appear in $CF_2{=}CH_2$. [In fact, Holmes *et al.*[27] have found that only about 78% of the total available energy in $\alpha\alpha$DF elimination in CH_2FCDF_2 goes to the $CH_2F\ddot{C}F$ ($\rightarrow CF_2{=}CH_2$) product.] Since this internal energy is much less than the 66 kcal/mol activation energy[24] for HF elimination in Eq. (20), the $:CHF + CH_2F_2$ reaction cannot contribute to the observed $HC{\equiv}CF$ production.

Some acetylene photoproduct is observed with yields of 2%–7% of the monofluoroacetylene yield; pyrolysis of difluoromethane also produces some acetylene.[24] C_2H_2 can be formed by the reaction of CHF radicals with 1,1-difluoroethylene [from Reactions (18) and (19)] to yield a transient 1,1,2-trifluorocyclopropane species. The $c\text{-}C_3H_3F_3^{\dagger}$ has about 72 kcal/mol of internal energy,[25] and rapidly decomposes to produce acetylene and other minor products. It should be noted that at 820 °C the CHF + 1,1-difluoroethylene reaction rate constant was measured to be 30 times larger than that for the $CHF + CH_2F_2$ reaction [Eq. (18)].[24] Due to the small amounts of observed 1,1-difluoroethylene (which never exceeded 3% of the monofluoroacetylene yield) and of observed acetylene, less than 9% of the MPD-produced CHF [Eq. (16)] fail to recombine to produce monofluoroacetylene. Therefore, Reaction (18) is not very important, and Eqs. (16) and (17) well describe the kinetics.

IV. EXPERIMENTAL RESULTS AND ANALYSIS

A. Deuterium optical selectivity in absorption

In previous investigations, a single-step deuterium enrichment factor (dissociation selectivity) of $\beta \sim 1000$ has been obtained in Freon 123[8] and $\beta \geq 5000$ has been measured in trifluoromethane.[10,11] However, efficient utilization of photons in photochemical deuterium separation can only be determined from knowledge of the deuterium optical selectivity in absorption (to be discussed in this subsection) and not the deuterium dissociation selectivity, which is characterized by β (to be discussed in Sec. IV C). Nevertheless, the dissociation selectivity is important in determining working molecule makeup requirements. Both makeup costs and photon utilization will be discussed in greater detail in Sec. V.

The absorption coefficient $\alpha(\phi)$ can be determined by integration of the expression for differential absorption (p = pressure, z = path coordinate)

$$\frac{d\phi}{\phi} = -\alpha(\phi) p\, dz \qquad (21)$$

provided the functional dependence of α on fluence ϕ is known. In this study, $\alpha(\phi)$ is modeled as a function of the fluence raised to the power $-\rho$:

$$\alpha(\phi) = A\phi^{-\rho} \ , \qquad (22)$$

where A is a constant. If α is assumed to be independent of fluence ($\rho = 0$), the familiar Beer's law results from integration of Eqs. (21) and (22):

$$\alpha(\phi_{\mathrm{in}}) = -\frac{1}{pl} \ln\left(\frac{\phi_{\mathrm{out}}}{\phi_{\mathrm{in}}}\right) \ , \qquad (23a)$$

where p is the partial pressure of the absorbing gas in the cell, l is the absorption cell length, ϕ_{out} is the transmitted peak fluence, and ϕ_{in} is the incident fluence. Since a collimated beam is used, the ratio $\phi_{\mathrm{out}}/\phi_{\mathrm{in}}$ is given by the ratio of input and transmitted CO_2 laser pulse energies.

Equation (23a) is exact when $\alpha(\phi)$ is independent of fluence, but overestimates the absorption coefficient when the absorption cross section decreases with increasing fluence. As is discussed further in Appendix A, for the deuterated molecules evaluated in this study this results in a correction that typically lowers $\alpha(\phi_{\mathrm{in}})$ by about 10% from that given by Eq. (23a) if a flat transverse laser beam profile is assumed.

A second correction must be made because the employed beam has a Gaussian transverse profile, in which more fractional absorption occurs in the wings of the beam, where the absorption coefficient $\alpha(\phi)$ is larger, than in the center of the beam. This second correction

TABLE II. Absorption measurement parameters using 2 ns CO_2 laser pulses.

				Representative conditions	
Primary gas	Secondary gas	CO_2 laser line[a]	Incident fluence[b] (J/cm^2)	Transmission[c]	$\alpha \times 10^{+3}$ (Torr^{-1} cm^{-1})[d]
100. Torr CF_3CHCl_2	0.0 Torr CF_3CDCl_2	$P(26)$	3	0.185	0.139
1.89 Torr CF_3CDCl_2		$P(26)$	3	0.20	7.0
1.47 Torr CF_3CDCl_2	50.1 Torr CF_3CHCl_2	$P(26)$	3	0.082	9.2
1.96 Torr CF_3CDCl_2		$P(20)$	3	0.27	5.7
0.98 Torr CF_3CDCl_2		$P(20)$	3	0.545	5.3
652 Torr CHF_3[e]		$P(20)$	1	0.95	0.00067
764 Torr CHF_3[e]		$R(16)$	1	0.83	0.0021[g]
730 Torr CHF_3[e]		$R(26)$	1	0.81	0.0024[g]
1.10 Torr CDF_3		$R(16)$	1	0.96	0.4
5.37 Torr CDF_3		$R(12)$	1	0.83	0.29
5.37 Torr CDF_3		$R(16)$	1	0.77	0.41
5.37 Torr CDF_3		$R(20)$	1	0.85	0.26
5.37 Torr CDF_3		$R(26)$	1	0.77	0.41
3.51 Torr CDF_3	164.7 Torr CHF_3[e]	$R(26)$	1	0.26	3.2
1.65 Torr CDF_3	768 Torr CHF_3[e]	$R(26)$	1	0.22	6.8
2.47 Torr CDF_3	111 Torr argon	$R(26)$	1	0.70	1.25
2.13 Torr CDF_3	780 Torr argon	$R(26)$	1	0.36	4.1
5.9 Torr $CHDF_2$	12.6 Torr CH_2F_2[f]	$P(8)$	0.5	0.073	3.8
5.9 Torr $CHDF_2$	12.6 Torr CH_2F_2[f]	$P(10)$	1	0.25	2.0
5.9 Torr $CHDF_2$	12.6 Torr CH_2F_2[f]	$P(14)$	1	0.42	1.25
7.3 Torr $CHDF_2$	15.7 Torr CH_2F_2[f]	$P(10)$	1	0.21	1.8
7.3 Torr $CHDF_2$	15.7 Torr CH_2F_2[f]	$P(12)$	1	0.40	1.08
7.3 Torr $CHDF_2$	15.7 Torr CH_2F_2[f]	$P(14)$	1	0.34	1.25
7.3 Torr $CHDF_2$	15.7 Torr CH_2F_2[f]	$P(16)$	1	0.39	1.1
7.3 Torr $CHDF_2$	15.7 Torr CH_2F_2[f]	$P(20)$	1	0.43	1.0
1005 Torr CH_2F_2[e]	0.3 Torr $CHDF_2$[e]	$P(8)$	0.5	0.61	0.0029
1005 Torr CH_2F_2[e]	0.3 Torr $CHDF_2$[e]	$P(10)$	1	0.70	0.0025
1005 Torr CH_2F_2[e]	0.3 Torr $CHDF_2$[e]	$P(12)$	1	0.73	0.0023
1005 Torr CH_2F_2[e]	0.3 Torr $CHDF_2$[e]	$P(14)$	1	0.78	0.0017
1005 Torr CH_2F_2[e]	0.3 Torr $CHDF_2$[e]	$P(16)$	1	0.77	0.0019
1005 Torr CH_2F_2[e]	0.3 Torr $CHDF_2$[e]	$P(18)$	1	0.78	0.0018
1005 Torr CH_2F_2[e]	0.3 Torr $CHDF_2$[e]	$P(20)$	1	0.78	0.0018

[a] 001–100, 10.4 μ band.

[b] Peak of Gaussian beam profile; fluence on axis.

[c] Bulk transmission based on absorption of all gases for a 118 cm cell length.

[d] Absorption coefficient for the primary gas ±10%.

[e] Natural deuterium isotopic abundance.

[f] 6% of this value is CD_2F_2; 780 Torr of argon buffer is also present.

[g] Uncorrected for absorption of naturally occurring CDF_3.

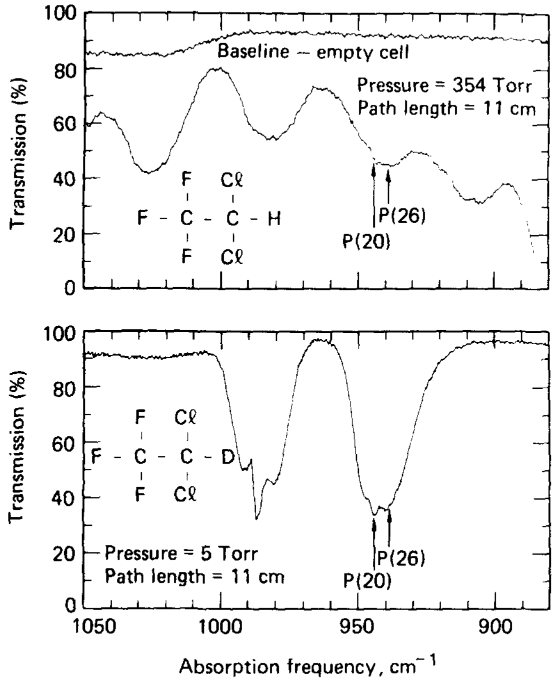

FIG. 4. The linear absorption spectrum of CF_3CHCl_2 (upper trace) and CF_3CDCl_2 (lower trace). The pressure of the upper trace is 75 times that of the lower trace to show weak absorption features. Note the two strong isotopically selective CF_3CDCl_2 bands at 944 and 987 cm^{-1}.

has been previously discussed in the literature[28] and is described in more detail in Appendix A; it amounts to approximately a 10%–30% further decrease in $\alpha(\phi_{in})$ for the deuterated species.

When these corrections are simply applied sequentially, they tend to only slightly overestimate the true correction to $\alpha(\phi_{in})$ (when compared to an exact treatment of beam absorption). The resulting modification to Beer's law results in the more exact expression [from Appendix A, Eq. (A9)]

$$\alpha(\phi_{in}) = \frac{1-\rho}{\rho l p}\left[1-\left(\frac{\phi_{out}}{\phi_{in}}\right)^{\rho}\right] . \qquad (23b)$$

In the limit of $\rho \rightarrow 0$, Eq. (23b) reduces to exactly Beer's law [Eq. (23a)]. The simple model of Eq. (22) is easily applied to the experimental data via Eq. (23b) only in fluence regimes where ρ is constant.

$\alpha(\phi)$ for Freon 123, difluoromethane, and trifluoromethane are reported below based on the experimental conditions indicated in Table II. The raw data is plotted in Figs. 5, 7–9, 11, and 12 using a Beer's law fit [Eq. (23a)]. The resulting absorption coefficient is plotted with an abscissa equal to the peak input fluence, so this uncorrected data actually represents $\alpha(\phi_{in})$. Since α determined in this manner is essentially fluence independent for the protonated species, the described correction is not required for these molecules. However, the correction is quite important for the deuterated molecules, and the corrected α is explicitly plotted for CDF_3 in Fig. 7 and discussed for CDF_3 and CF_3CDCl_2 in the text (see also Figs. 19 and 20). When Eq. (23b) is applied in the high fluence regime, the obtained absorption coefficient is typically 30%–40% (~20% in CF_3CDCl_2) lower than the reported value calculated using Beer's law. Note that when either the corrected or a fluence independent α is plotted, the abscissa represents the local fluence—and not the peak input fluence. Also, unless otherwise specified, each presented graph which displays the absorption coefficient of either a deuterated or protonated molecule has been corrected for residual absorption due to any added (secondary) gas.

1. 2,2-Dichloro-1,1,1-trifluoroethane

The linear absorption of CF_3CDCl_2 and CF_3CHCl_2 as measured by conventional infrared spectroscopy is shown in Fig. 4. The CF_3CHCl_2 sample used for the data in Fig. 4 was specially purified to contain less than 0.05% $CF_2ClCHFCl$ isomer impurity (Freon 123a). Also, note that in this diagram the CF_3CHCl_2 pressure was 75 times higher than that employed for CF_3CDCl_2, to more easily determine weak absorption in CF_3CHCl_2 near 10.2 and 10.6 μ where CF_3CDCl_2 has absorption peaks (C–D bends). Nielsen *et al.*[29] have made vibrational transition identifications of the weak CF_3CHCl_2 peaks near 10 μ in a sample of unspecified purity. Based upon the linear absorption data of Fig. 4, the deuterium isotopic selectivity in linear absorption, defined as the ratio $\alpha_D(\lambda)/\alpha_H(\lambda)$, is 111± 5 at 944 cm^{-1} [near the $P(20)$ CO_2 laser line wavelength] and 99± 5 at 939 cm^{-1} [~$P(26)$ CO_2 laser line]. The maximum Freon 123 deuterium optical selectivity in linear absorption occurs for the 10.2 μ peak and is 157± 8 at 987 cm^{-1} [~$R(38)$ CO_2 laser line]. Recent measurements of Freon 123 deuterium optical selectivity using 1 μs duration laser pulses at $P(20)$, 10.6 μ yield values of 65–100 at 0.2 J/cm^2, depending on pressure.[30] Similar values were measured at $R(28)$, 10.2 μ, where the optical selectivity was also found to be pressure sensitive.[30]

The absorption coefficient in CF_3CDCl_2 using 2 ns duration CO_2 laser pulses at the $P(20)$ and $P(26)$ CO_2 laser lines is shown as a function of peak incident fluence in Fig. 5 (see Table II). Figure 5 shows that absorption in pure CF_3CHCl_2 is essentially constant as a function of fluence, and that absorption in CF_3CHCl_2 is slightly stronger at $P(26)$ than at $P(20)$. The effect of addition of 50 Torr of CF_3CHCl_2 to CF_3CDCl_2 is shown in the top trace of Fig. 5, and indicates a slight enhancement in the measured absorption. As discussed in Sec. V.A, this can be due to two contributions—enhanced absorption due to collisional hole filling in low lying levels in CF_3CDCl_2, and collisional funneling of energy into CF_3CHCl_2 following initial absorption in CF_3CDCl_2. Since there is only a slow falloff in the raw data plot of α vs ϕ, aberrations from Beer's law are not very severe (~20%). The corrected α for neat CF_3CDCl_2 with the $P(26)$ laser line may be expressed as $\alpha(\phi) = 6.7 \times 10^{-3}/\phi^{0.12}$ (cm^{-1} $Torr^{-1}$) for $0.005 < \phi < 5$ (all ϕ in J/cm^2). Based on the measured absorption coefficients, Fig. 5 shows that the deuterium optical selectivity in absorption for 50 Torr of Freon 123 at 5 J/cm^2 fluence (where significant dissociation is beginning to occur) is only about 59 for the $P(26)$ CO_2 laser line. This is about half the low fluence value, and is over an order of magnitude too low for viable photochemical separation (see Sec. V B).

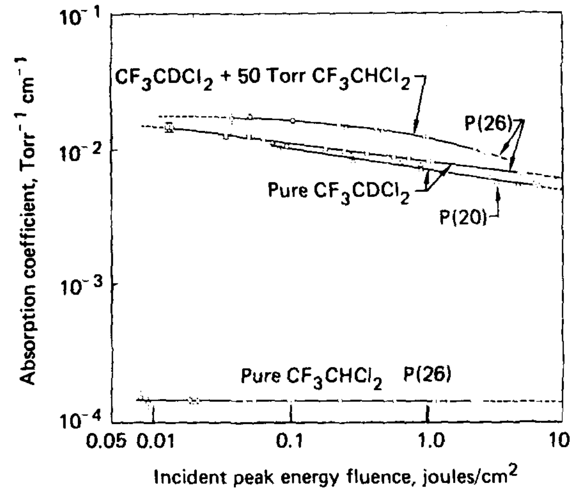

FIG. 5. The absorption coefficient of Freon 123 measured using 2 ns duration CO_2 laser pulses is displayed as the incident fluence is varied. The upper traces are for CF_3CDCl_2 buffered by 50 Torr CF_3CHCl_2 at $P(26)$ (topmost trace), pure CF_3CDCl_2 at $P(26)$ (middle upper trace), pure CF_3CDCl_2 at $P(20)$ (lowest upper trace), and 100 Torr pure CF_3CHCl_2 at $P(26)$ (lowermost trace).

Both trifluoromethane and difluoromethane have much higher deuterium selectivity in absorption, as shown in the next subsections.

2. *Trifluoromethane*

The wavelength dependence of linear absorption of CDF_3 and CHF_3 measured with an infrared spectrometer using 10 cm long absorption cells is shown in Fig. 6. Two selective peaks in CDF_3 absorption ($\nu_5 \leftarrow 0$) appear near 10.2 and 10.3 μ in Fig. 6, which also shows weak absorption features in CHF_3 ($2\nu_6 \leftarrow 0$) near 9.9 μ.[31] The CHF_3 absorption depicted in Fig. 6 was measured at 100 times higher pressure than used for CDF_3, since accurate measurement of very weak CHF_3 absorption is needed to determine the linear isotopic selectivity in absorption near 970 and 980 cm^{-1}. The CHF_3 sample used in Fig. 6 had a deuterium abundance of 150± 10 ppm.[21] Even with a high pressure of CHF_3, very little optical absorption in the CHF_3 sample can be determined based on the data of Fig. 6. At 980 cm^{-1} the linear CDF_3 absorption coefficient is 1.0×10^{-2} Torr^{-1} cm^{-1} at room temperature, corresponding to a deuterium optical selectivity in absorption of 3000–8000; at 970 cm^{-1} the linear CDF_3 absorption coefficient is 0.9×10^{-2} Torr^{-1} $\times$ cm^{-1} at room temperature, corresponding to an even larger deuterium optical selectivity in absorption of 4000–20 000. Inaccuracies inherent in trying to measure the small amount of CHF_3 absorption at 970 and 980 cm^{-1} using 10 cm long cells prevent a more accurate measurement of linear deuterium optical selectivity in absorption.

CDF_3 optical absorption at 979.7 cm^{-1} [$R(26)$ CO_2 laser line] was measured using 2 ns duration pulses, since such short pulse durations are anticipated to be necessary in a working process for photochemical deuterium separation at operating pressures of 0.1–0.5 atm. The CDF_3 absorption coefficients calculated from Eq. (23a) are plotted in Fig. 7 for various values of the peak incident fluence (see also Table II). The bottom curve in Fig. 7 shows that the absorption in pure CDF_3 (no added secondary gas) falls strongly with increasing fluence, and at 1 J/cm^2 fluence it is 25 times weaker than the linear absorption coefficient. Absorption above 0.1 J/cm^2 fluence is enhanced by a factor of 3 with 111 Torr of added argon (middle curve) and by fully tenfold with 780 Torr of argon secondary gas, as shown in the top curve of Fig. 7. Note that for the top curve (1 atm added argon) the CDF_3 absorption coefficient remains constant below about 0.2 J/cm^2 fluence, asymptotically approaching a value of $(1.05\pm0.05)\times10^{-2}$ Torr^{-1} cm^{-1} in the low fluence or linear absorption regime. It is clear from the large increase in absorption coefficient with added argon shown in Fig. 7 that collisions are an extremely important factor in permitting significant CDF_3 absorption, and hence in allowing decomposition by infrared multiple-photon dissociation.[9] This observation is discussed further in Sec. V A.

The raw data was corrected using the procedure outlined in Appendix A for both the neat CDF_3 and the CDF_3/780 Torr Ar mixture samples. The resulting absorption coefficient information calculated using Eq. (23b) is plotted as the thin lines on Fig. 7, and can be represented by the formulas for neat CDF_3: $\alpha(\phi)=2.5\times10^{-4}/\phi^{0.35}$ (cm^{-1} Torr^{-1}) for $\phi < 0.3$ J/cm^2; and for the CDF_3/780 Torr Ar mixture: $\alpha(\phi)=2.75\times10^{-3}/\phi^{0.28\pm0.02}$ (cm^{-1} $\times$ Torr^{-1}) in the range $0.3 < \phi < 1.2$ J/cm^2 (all ϕ in J/cm^2).

In an actual photochemical deuterium separation process, small amounts of CDF_3 will be present with a large excess of CHF_3, since the CDF_3 natural abundance is typically 150 ppm.[21] The effect of CHF_3 collisions on CDF_3 absorption was measured, and is displayed in Fig. 8. The lower curve of Fig. 8 is the curve for absorption in neat CDF_3, which is also presented in Fig. 7. The upper two curves display the CDF_3 absorption as a func-

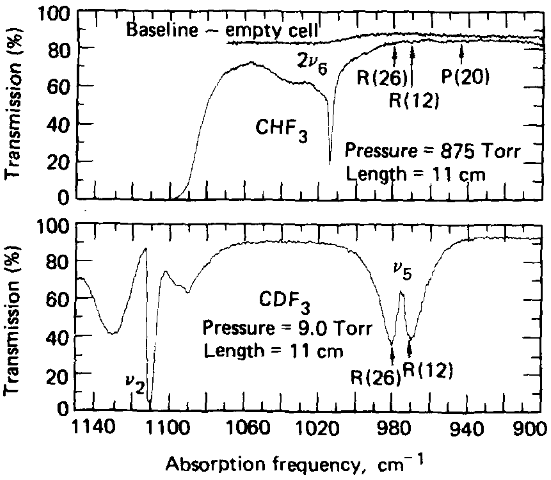

FIG. 6. The linear absorption for CHF_3 is displayed in the upper trace and for CDF_3 in the lower trace. The upper trace is at 100 times higher pressure than the lower trace to enhance weak absorption features, such as the CHF_3 $2\nu_6$ overtone band at 1013 cm^{-1}. Highly deuterium selective absorption occurs in CDF_3 at 970 and 980 cm^{-1}, shown in the lower trace.

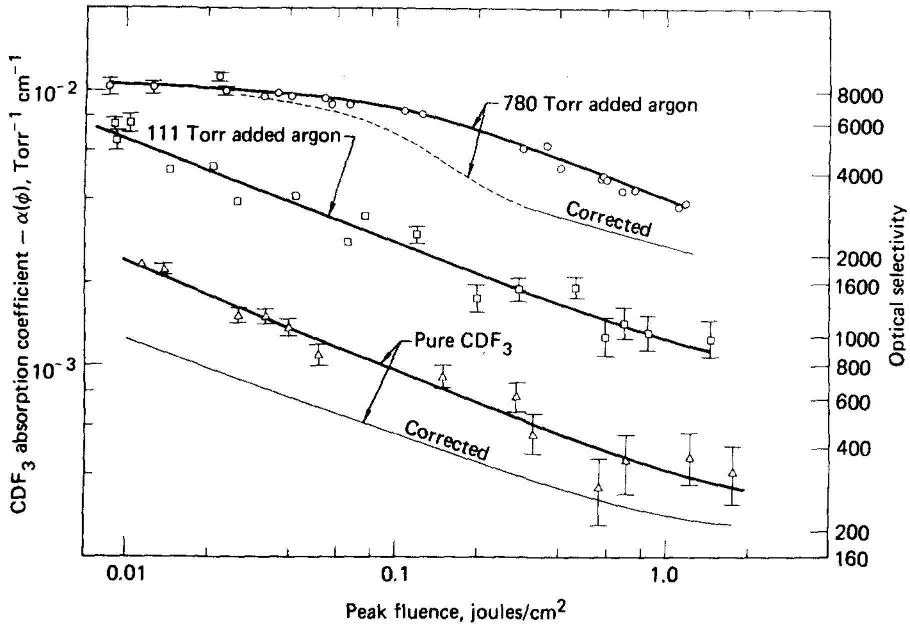

FIG. 7. The absorption coefficient of CDF_3 determined by 2 ns duration CO_2 laser pulses at $R(26)$, 10.21 μ is shown as a function of peak laser energy fluence. The upper two traces show CDF_3 absorption buffered by 780 Torr of added argon; the thick curve is obtained using Beer's law and the thin curve is corrected according to Eq. (A9). The middle curve shows CDF_3 absorption buffered by 111 Torr added argon. The lower two curves show neat CDF_3 absorption; the thick line is from Beer's law and the thin line is corrected according to Eq. (A9). For the data corrected using Eq. (A9) the abscissa denotes the local fluence, and not the peak beam fluence. Note the D/H optical selectivity scale on the right ordinate axis.

tion of peak incident fluence for 165 and 768 Torr of added CHF_3.

Comparison of Figs. 7 and 8 indicates that the net absorption in CDF_3 is enhanced even more by CHF_3 collisions than by collisions with argon at the same secondary gas pressure. Whereas CDF_3 absorption is independent of fluence below about 0.2 J/cm^2 with 1 atm of added argon, the linear absorption regime extends to three times higher fluence in CDF_3 with 1 atm of added CHF_3. The CDF_3 absorption experiments are summarized in Table II, which indicates that the net CDF_3 absorption coefficient at 1 J/cm^2 is enhanced eight times with 165 Torr added CHF_3, and is enhanced 16 times with 1 atm of added CHF_3.

In the high fluence regime above about 0.5 J/cm^2 (but below those fluences at which significant dissociation takes place), the CDF_3 absorption coefficient may be estimated assuming a linear extrapolation of the appropriate corrected data graph on the log–log plots in Fig. 7, or equivalently by utilizing the algebraic representation presented above (see also Sec. V A).

The absorption in natural isotopic abundance trifluoromethane was measured at the $P(20)$, $R(16)$, and $R(26)$ 10.4 μ band CO_2 laser lines, as indicated in Table II. The data for $R(16)$ and $P(20)$ are illustrated in Fig. 9 and are uncorrected for the presence of naturally occurring CDF_3. Since CDF_3 does not absorb at $P(20)$, 944 cm^{-1} (see Fig. 6), the $P(20)$ data accurately reflects the intrinsic CHF_3 absorption at 10.6 μ. As indicated in Table II, only about 5% absorption occurred at $P(20)$ over a 118 cm path length at 652 Torr CHF_3. This small measured absorption accounts for the large uncertainties in the $P(20)$ data shown in Fig. 9, since the measured 5% ab-

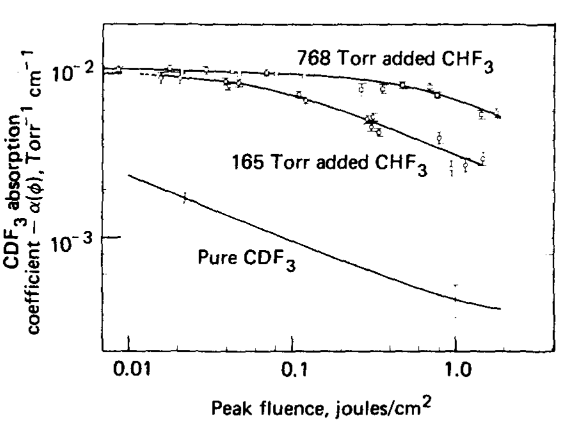

FIG. 8. The CDF_3 absorption coefficient obtained using 2 ns duration CO_2 laser pulses at $R(26)$, 10.21 μ is shown as a function of peak laser energy fluence. The curves show CDF_3 absorption buffered by 768 Torr CHF_3 (upper trace), buffered by 165 Torr CHF_3 (middle trace), and neat CDF_3 absorption (lower trace). CHF_3 absorption has been subtracted from the upper two curves.

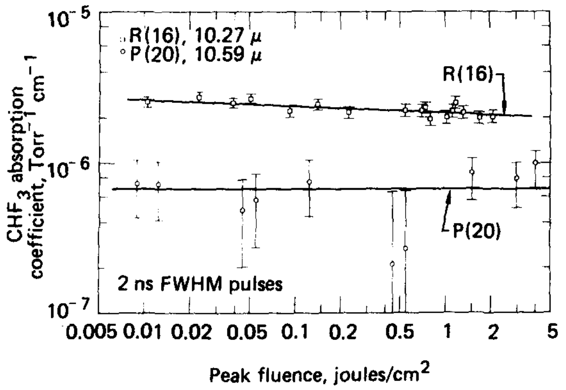

FIG. 9. The absorption coefficient of natural trifluoromethane using 2 ns duration laser pulses is shown as a function of peak laser energy fluence. The upper trace was taken for the $R(16)$, 10.27 μ laser line (764 Torr trifluoromethane) and the lower trace was taken for the $P(20)$, 10.59 μ laser line (652 Torr trifluoromethane). The curves indicate the total absorption coefficient due to both CHF_3 and naturally occurring CDF_3 ($\delta \sim 150$ ppm). The trifluoromethane absorption coefficient at $R(26)$, 10.21 μ is 10%–20% higher than at $R(16)$, 10.27 μ.

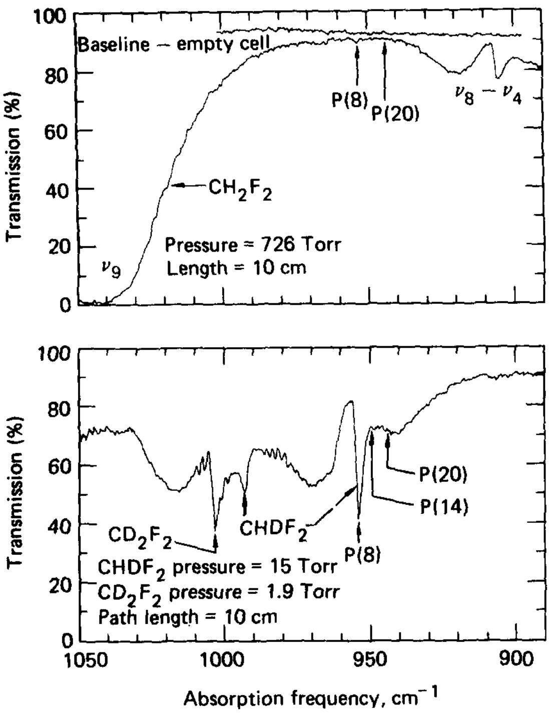

FIG. 10. The linear absorption of CH_2F_2 is displayed in the upper trace and $CHDF_2$ linear absorption is displayed in the lower trace. The strong peak at 1003 cm^{-1} is due to the 2 Torr of CD_2F_2 present in the sample. The upper trace is at 50 times higher pressure to enhance weak absorption features. Highly deuterium selective absorption occurs in $CHDF_2$ at 954 cm^{-1}. The weak peak at 954 cm^{-1} in the upper trace is due to the 0.3% naturally occurring $CHDF_2$.

sorption is comparable to the ~3% transmission measurement accuracy achievable by this particular technique of calorimetric absorption; there is relatively less scatter in the data at $R(16)$. At each measured fluence the absorption cross section at $R(26)$, 10.2 μ is about 10% higher than with the $R(16)$ laser line. The actual absorption coefficient due only to CHF_3 may be determined from the data of Fig. 8 by subtracting the absorption due to naturally occurring CDF_3 buffered by 1 atm of CHF_3. From Table II, the measured absorption coefficient of 730 Torr natural isotopic abundance trifluoromethane at the $R(26)$, 10.2 μ CO_2 laser line is $\alpha_{\rm meas} = (2.4 \pm 0.3)\times 10^{-6}$ Torr^{-1} cm^{-1} at room temperature at 1 J/cm^2 peak incident fluence. From Table II and Fig. 8 the corresponding CDF_3 absorption coefficient buffered by 768 Torr of CHF_3 is $\alpha_D = (6.8 \pm 0.6)\times 10^{-3}$ Torr^{-1} cm^{-1} at $R(26)$. Since the trifluoromethane used in these measurements has a natural CDF_3 content of approximately $\delta = 150$ ppm,[21] the true intrinsic absorption coefficient of CHF_3, i.e., α_H, may be calculated from the expression

$$\alpha_{\rm meas} = \alpha_H + \delta\alpha_D \ , \qquad (24)$$

yielding a CHF_3 absorption coefficient at $\phi = 1$ J/cm^2 of $\alpha_H = (1.4 \pm 0.3)\times 10^{-6}$ Torr^{-1} cm^{-1} at 10.21 μ.

The optical isotopic selectivity in absorption $S(\phi)$ is simply equal to α_D/α_H, leading to $S(\phi) = 4900 \pm 1200$ for trifluoromethane at $R(26)$, 10.2 μ at 1 J/cm^2 peak incident fluence. The optical selectivity is even larger near 10.3 μ and also at lower fluences. This is about two orders of magnitude larger than for Freon 123, and indicates that relatively good photon utilization may be achievable in deuterium separation by photodissociation of natural trifluoromethane. This will be analyzed in greater detail in Sec. V.

3. *Difluoromethane*

The linear absorption spectra of CH_2F_2[32,33] and of $CHDF_2$ measured with an infrared spectrometer are shown in Fig. 10. This is the first published IR spectrum of $CHDF_2$. A strong Q-branch peak due to $CHDF_2$ is indicated at 954 cm^{-1} (CHD twist) in a spectral region where CH_2F_2 is very transparent. The absorption of CH_2F_2 was measured at 50 times higher pressure than used for $CHDF_2$ to bring out weak absorption features; a weak CH_2F_2 hot band with Q-branch peak at 905 cm^{-1} $(\nu_8-\nu_4)$[32,33] can be discerned. The tail of the strong CH_2F_2 $\nu_9(b_2)$ fundamental mode dominates CH_2F_2 absorption near 1000 cm^{-1}. Since the $CHDF_2$ sample was prepared by isotopic exchange as described in Sec. II B, the statistical distribution of a sample containing 20% deuterium resulted in ~4% CD_2F_2, which is characterized by a strong absorption band at 10.0 μ[33] indicated by the Q-branch peak at 1003 cm^{-1} $[\nu_9(b_2)]$.[33] The weaker absorption feature at 993 cm^{-1} is a Q-branch peak for another $CHDF_2$ mode. The broad feature at ~1017 cm^{-1} is due to CD_2F_2, and the broad features at ~970 and 940 cm^{-1} belong to the 954 cm^{-1} $CHDF_2$ mode.

Based on the linear absorption spectra of Fig. 10, $CHDF_2$ has a peak absorption coefficient of $\alpha_D = (5.2 \pm 0.4)\times 10^{-3}$ Torr^{-1} cm^{-1} at 954 cm^{-1} at room temperature. A deuterium natural abundance of 150 ppm means that natural difluoromethane will contain 0.03% $CHDF_2$, corresponding to a 0.22 Torr $CHDF_2$ contribution to the difluoromethane absorption spectrum shown in the top of Fig. 10, where the weak naturally occurring $CHDF_2$ absorption peak is just visible under the arrow marked $P(8)$. Using Eq. (24) with $\delta = 3\times 10^{-4}$ and the weak measured CH_2F_2 absorption portrayed in Fig. 10, the $CHDF_2$ deuterium optical selectivity in absorption is 2000^{+2000}_{-700} at 954 cm^{-1} at room temperature. The indicated range of 1300–4000 in $CHDF_2$ deuterium optical selectivity at 954 cm^{-1} is due to the inability to accurately measure from Fig. 10 the very weak absorption occurring in natural isotopic abundance difluoromethane. Considerably greater accuracy was obtained using a 12 times longer absorption cell length for the calorimetric absorption measurements described next using 2 ns duration CO_2 laser pulses.

The $P(8)$, 10.5 μ CO_2 laser line at 954.5 cm^{-1} is well matched to the $CHDF_2$ linear absorption feature at this frequency, and was used to probe $CHDF_2$ absorption as a function of peak incident laser fluence. This data is plotted in Fig. 11, using Eq. (23a) to evaluate the room temperature absorption coefficient α_D. Figure 11 also shows the fluence dependence of the $CHDF_2$ absorption coefficient at the $P(10)$ and $P(14)$ laser lines. Measured absorption coefficients were nearly equal at the $P(12)$, $P(16)$, and $P(20)$ lines, as is also indicated in this figure. Table II summarizes the experimental conditions

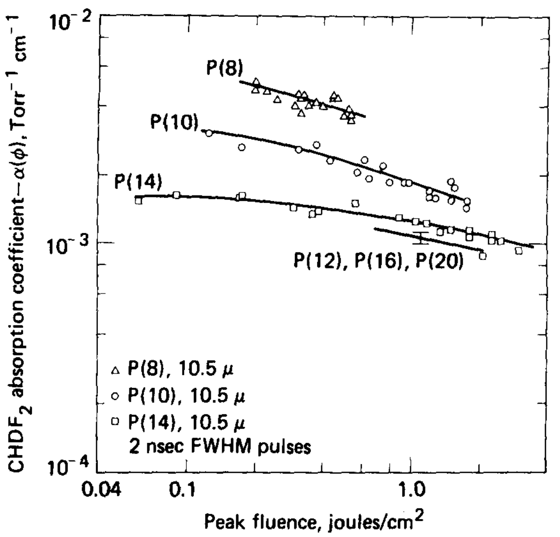

FIG. 11. The absorption coefficient of $CHDF_2$ measured by 2 ns duration CO_2 laser pulses buffered by 780 Torr argon is shown as a function of peak laser energy fluence. $CHDF_2$ absorption is shown for $P(8)$, 10.48 μ (upper trace); $P(10)$, 10.49 μ (below upper trace); and $P(14)$, 10.53 μ (above lowest trace). Absorption at $P(12)$, $P(16)$, and $P(20)$ is similar, and indicated in the bottom trace.

used to obtain the data of Fig. 11, and indicates that for all measurements 780 Torr of argon buffer gas was added to achieve rotational hole filling and thus facilitate absorption of the laser energy. As was shown for the case of CDF_3 absorption (see Figs. 7 and 8), significantly enhanced absorption of 2 ns duration laser pulses occurs with ≥ 1 atm of secondary buffer gas. Because of the reduced performance of the mode-locked CO_2 laser at the $P(8)$ laser line, absorption measurements were only feasible to a maximum fluence of 0.5 J/cm². In contrast, $CHDF_2$ absorption measurements at $P(14)$ were measured up to a peak incident fluence of 3 J/cm². The data of Fig. 11 also indicates the characteristic weakening of molecular absorption coefficient α_D with increasing incident laser fluence.

Because of weak anticipated absorption in natural difluoromethane near 10.5 μ, the 118 cm long absorption cell was filled with more than atmospheric pressure, specifically 1005 Torr of CH_2F_2, which contained an assumed natural isotopic contribution of 0.3 Torr $CHDF_2$. Natural difluoromethane absorption was measured using the $P(8)$ through $P(20)$ CO_2 laser lines resulting in the data summarized in the bottom of Table II. For all examined CO_2 laser lines, with the possible exception of $P(14)$, an unexpected consistent *increase* in the CH_2F_2 absorption coefficient with increasing laser fluence was measured. Using Eq. (24) and assuming $\delta = 3\times10^{-4}$, the CH_2F_2 absorption coefficient α_H was computed, and is plotted in Fig. 12 as a function of peak incident laser fluence for the representative $P(8)$, $P(10)$, and $P(18)$ CO_2 laser lines. Note that in obtaining α_H it has been assumed that the $CHDF_2$ absorption coefficient α_D, as given in Fig. 11, could be used, although in this case the "secondary" buffer gas was 1.3 atm of CH_2F_2, and not the 1.0 atm of argon used for obtaining Fig. 11. Based on the trifluoromethane data of Figs. 7 and 8, it appears that the $CHDF_2$ absorption coefficient will be somewhat higher with CH_2F_2 as buffer, compared to using argon. Hence, the α_D term used in Eq. (24) may be too small, and the data of Fig. 12 may slightly overestimate the true intrinsic CH_2F_2 absorption coefficient α_H; consequently, S, the optical selectivity, may be underestimated. Since the plots of the absorption coefficient of CH_2F_2 at $P(12)$, $P(14)$, $P(16)$, and $P(20)$ are parallel to those presented in Fig. 12, $\alpha(\phi)$ may be determined at each wavelength by using the value of α quoted for $\phi = 1$ J/cm² in Table II.

TABLE III. Deuterium optical selectivity in difluoromethane absorption near 10.5 μ.

CO_2 laser line[a]	Fluence[b] (J/cm²)	Isotopic selectivity[c]
$P(8)$	0.2	1800 ± 300
	0.5	1250 ± 200
$P(10)$	0.2	1400 ± 200
	1.0	740 ± 200
$P(12)$	1.0	500 ± 100
$P(14)$	0.2	1000 ± 150
	1.0	800 ± 150
$P(16)$	1.0	580 ± 100
$P(18)$	1.0	600 ± 100 estimated
$P(20)$	1.0	560 ± 100

[a] 001–100, 10.4 μ band.
[b] Peak incident fluence on axis.
[c] Deuterium optical selectivity in absorption, determined from the α_D/α_H ratio, calculated from Beer's law [Eq. (23a)].

Based on the data shown in Figs. 11 and 12, the $CHDF_2$ optical selectivity in absorption may be determined from the α_D/α_H ratio for each value of the laser fluence and laser frequency. Several values are tabulated in Table III for the $P(8)$–$P(20)$ CO_2 laser lines. Examination of this data indicates that the highest $CHDF_2$ deuterium optical selectivities in absorption occur for the $P(8)$, $P(10)$, and $P(14)$ CO_2 laser lines. Except for the $P(14)$ line, this is consistent with the linear absorption data shown in Fig. 10. As expected, Table III indicates that the isotopic selectivity is decreasing with increasing fluence. Since significant $CHDF_2$ dissociation occurs only above about 10 J/cm², the working

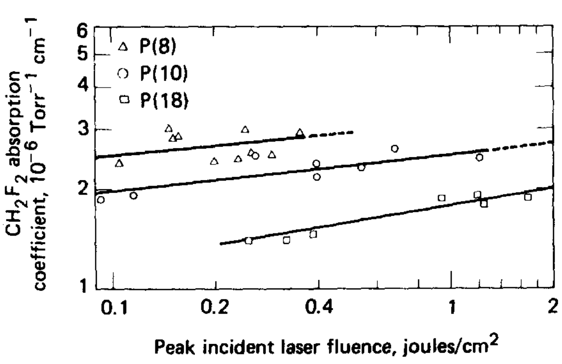

FIG. 12. The absorption coefficient of CH_2F_2 as probed by 2 ns duration CO_2 laser pulses is shown as a function of peak laser fluence. CH_2F_2 absorption is shown for $P(8)$, 10.48 μ (upper trace); $P(10)$, 10.49 μ (middle trace); and $P(18)$, 10.57 μ (lower trace). Data were taken at 1005 Torr, with $CHDF_2$ absorption subtracted using the data of Fig. 11.

deuterium optical selectivity in absorption will be perhaps half as large as the values indicated in Table III for an actual photochemical deuterium separation process using difluoromethane. However, since difluoromethane carries two potential deuterium sites per molecule, the abundance of the naturally occurring species is doubled from the natural deuterium content (to about 0.03% $CHDF_2$), and the photon utilization is improved compared to a monohydrogenated molecule, such as trifluoromethane. This is equivalent to effectively doubling the difluoromethane optical selectivity in a comparison with trifluoromethane. These matters are discussed in greater detail in Sec. V B.

B. Photoproduct yield

The essential issue of whether deuterium separation is practical at high pressure can be examined from the photoproduct yield dependence on pressure. Even though deuterium enrichment may be high at a given operating pressure, deuterium separation is not practical unless the photoproduct yield is also high ($\gtrsim\sim 0.5$) at the same pressure. The photoproduct yield is presently defined as the probability that a molecule within the beam will dissociate; a more quantitative characterization of the MPD probability is presented below. As has been suggested in the prior subsection, it may be preferable to add significant amounts of inert buffer gas to the deuterated species to facilitate absorption via removing the rotational bottlenecks which appear in IR photolysis of fluoromethanes.[9] Using nanosecond duration CO_2 laser pulses for dissociation, optimal energy absorption and decomposition yield should occur for buffer gas pressures of 1–3 atm. However, the most significant experiments for an investigation of deuterium separation consist of the measurement of the photoproduct yield of the deuterium-bearing species as the pressure of the hydrogen-bearing species of the same working molecule is increased. Therefore, the most critical pressure is that of the working molecule, e.g., difluoromethane, and not necessarily the total system operating pressure (which may include added buffer gases). The effect of adding the protonated molecules as a secondary gas has already been measured for CDF_3,[9] using 100 ns duration CO_2 laser pulses for dissociation; that study indicated that the C_2F_4 photoproduct yield is strongly quenched above 1 Torr of added CHF_3. It was expected that shortening the CO_2 laser pulse to 2 ns would strongly increase the permissible operating pressure; this has been verified as indicated below. In this study, preliminary data on the dissociation probability of CF_3CDCl_2, CDF_3, and $CHDF_2$ have been obtained for various fluences and various values of added pressure of either argon or of the corresponding nondeuterated molecule—CF_3CHCl_2, CHF_3, and CH_2F_2, respectively.

In order to meaningfully present the data, the raw data was first deconvoluted to determine the separate bulk yields of the deuterated and the protonated species, in cases where the normal species was added as a secondary gas. In addition, due to variations in the experimental conditions in different runs, all obtained data were then analyzed using a model which incorporates these variations. The employed procedure is outlined below.

Let δ equal the initial fraction of deuterium in the unreacted working gas, at pressure $R(0)$, containing initial partial pressure $R_D(0)$ of deuterated species and $R_H(0)$ of protonated species

$$\delta \equiv \frac{R_D(0)}{R_D(0)+R_H(0)} = \frac{R_D(0)}{R(0)} , \tag{25}$$

and let f_D define the fraction of deuterium in the final photoproduct at pressure P containing partial pressure P_D of deuterium bearing molecules according to

$$f_D \equiv \frac{P_D}{P} = \frac{\beta\delta}{1+\delta(\beta-1)} , \tag{26}$$

where β is the single-step deuterium enrichment factor defined in Eq. (1) and δ is the initial reactant deuterium fraction defined in Eq. (25).

Photoproduct yields are analyzed assuming that a fraction γ_D of deuterated reactant starting material at pressure R_D is decomposed per pulse. The partial pressure $R_D(n)$ of deuterated starting material after n pulses is determined by

$$\frac{dR_D}{dn} = -\gamma_D R_D , \tag{27}$$

$$R_D(n) = R_D(0)\, e^{-\gamma_D n} , \tag{28}$$

where $R_D(0)$ is the pressure of initial deuterium-containing reactant. Similarly, the pressure of protonated working molecule $R_H(n)$ after n pulses is given by

$$R_H(n) = R_H(0)\, e^{-\gamma_H n} , \tag{29}$$

where γ_H is the fraction of protonated (undeuterated) starting material at pressure R_H that decomposes per pulse, and $R_H(0)$ is the initial pressure of the protonated working molecule. γ_D/γ_H is the intrinsic molecular isotopic selectivity in dissociation, and is equal to or greater than the measured deuterium single-step enrichment factor β, depending on scrambling reactions.

Let x denote the number of deuterium-bearing reagent molecules that decompose to yield one molecule of deuterium-bearing photoproduct. Then the buildup of photoproduct pressure $P_D(n)$ after n pulses is given by

$$\frac{dP_D}{dn} = +\frac{1}{x}\gamma_D R_D , \tag{30}$$

$$P_D(n) = \frac{R_D(0)}{x}\left(1-e^{-\gamma_D n}\right) . \tag{31}$$

Dividing Eq. (31) by Eq. (28) and solving for γ_D yields

$$\gamma_D = \frac{1}{n}\ln\left(1+\frac{xP_D}{R_D}\right) . \tag{32}$$

After performing a little algebra P_D and R_D may be expressed in terms of P and R, where $R\ (\equiv R_H+R_D)$ denotes the remaining reactant:

$$\gamma_D = \frac{1}{n}\ln\left\{1+\frac{x\beta P}{[1+\delta(\beta-1)]R - x(1-\delta)(\beta-1)P}\right\} , \tag{33a}$$

$$\gamma_D \cong \frac{1}{n}\ln\left[1+\frac{xP}{(\delta+1/\beta)R}\right] , \quad \beta \gg 10 , \quad xP \ll \delta R . \tag{33b}$$

Equation (33) now expresses γ_D in terms of the measurable quantities β, P, and R assuming no isotopic scrambling (see Sec. III). The ratio P/R is the bulk yield and is directly determined from GC analysis using the sensitivity factors χ listed in Table I by the relation

$$\frac{P}{R}=\frac{A_P}{A_R\chi}\ , \tag{34}$$

where A_P is the area of the photoproduct peak and A_R is the area of the reactant peak, measured by GC after irradiation by n laser pulses.

γ_D and γ_H represent the fraction of the respective species in the gas cell that are decomposed per pulse, and therefore depend quite strongly on the cell size, the focusing geometry, and the laser energy. They may be converted into a much more useful form by calculating the dissociation probability—which is a molecular and not a geometric property.

The dissociation probability $D(\phi,\lambda)$ of a deuterium-bearing working molecule in the presence of a resonant infrared field of energy fluence ϕ and wavelength λ typically exhibits a cubic power law dependence on fluence below the saturation fluence ϕ_{sat}.[8,9] Using this characterization, the dissociation probability may be written as

$$D=D(\phi,\lambda)=(\phi/\phi_{sat})^3\ ,\quad \phi\le\phi_{sat}\ , \tag{35a}$$

$$=1\ ,\quad \phi>\phi_{sat}\ . \tag{35b}$$

This relation seems to hold reasonably well for dissociation of CDF_3 and CF_3CDCl_2, provided the fluence is greater than about $0.1\ \phi_{sat}$.[8,9] The (measured) fractional yield γ_D is then related to the dissociation probability D by the relation

$$\gamma_D=\frac{1}{V}\int_V D(\phi,\lambda)\,dV=\frac{1}{V}\int\!\!\int_V\!\!\int D(\phi,\lambda)r\,dr\,d\theta\,dz\ , \tag{36}$$

where V is the volume of the cylindrical reaction cell and r, θ, and z are the usual cylindrical coordinates.

Equation (36) has been integrated exactly for the case of a general power law dependence [Eq. (B1)] with an incident focused Gaussian beam.[34] The important and relevant details of this calculation have been outlined in Appendix B, along with a discussion of an extension of the Ref. 34 results to optically thick photolysis cells, and an explanation of other procedures and approximations employed in the data analysis. The expression given in Appendix B [Eq. (B6)], which includes laser absorption in the photolysis cell, is employed in data analysis in this study. For illustrative purposes the simplified versions for optically very thin media are now presented.

At fluences below saturation in optically thin samples the expression for the observed yield in terms of geometric and photochemical parameters is[34]

$$\gamma_D=\frac{\pi\omega_0^2 z_R}{6V}\left[\tan^{-1}\left(\frac{l}{2z_R}\right)+\frac{\dfrac{l}{2z_R}}{1+\left(\dfrac{l}{2z_R}\right)^2}\right]\eta^3\ ,\quad \eta\le 1 \tag{37}$$

where l is the cell length, ω_0 is the beam radius at the focus, z_R is the Rayleigh range (see Appendix B), and η is the ratio of the peak fluence at the focus to the saturation fluence

$$\eta=\frac{\phi(r=0,\ z=0)}{\phi_{sat}}\ . \tag{38}$$

Above saturation ($\eta>1$, optically thin sample) γ_D becomes

$$\gamma_D=\frac{\pi\omega_0^2 z_R}{6V}\Bigg[10(\eta-1)^{1/2}+2(\eta-1)^{3/2}-\eta^2(\eta-1)^{1/2}$$
$$-8\tan^{-1}(\eta-1)^{1/2}-\eta^3\tan^{-1}(\eta-1)^{1/2}+\eta^3\tan^{-1}\left(\frac{l}{2z_R}\right)$$
$$+\eta^3\frac{\dfrac{l}{2z_R}}{1+\left(\dfrac{l}{2z_R}\right)^2}\Bigg]\ ,\quad \eta\ge 1\ . \tag{39}$$

[Both Eqs. (37) and (39) are valid only for $\eta<1+(l/2z_R)^2$ (or $\eta<6.5$ in these experiments); see Appendix B or Ref. 34 for details.] These expressions are used after first calculating the fractional yield γ_D [Eq. (33)] based on the experimentally measured reactant and photoproduct peak heights using GC analysis. Then the corresponding values of η, and hence ϕ_{sat}, are determined using Eq. (B6) in Appendix B; and the dissociation probability at a standard fluence may then be calculated using Eq. (35), employing the values of ϕ_{sat} determined above. These expressions are finally used to compare the dissociation probabilities at various operating pressures for the three working gases, as detailed below.

As is clear from the discussion of the high intensity absorption coefficients of the molecules under study, collisions can have a large effect on multiple-photon absorption and MPD. Collisions during the laser pulse can either beneficially remove absorption bottlenecks or detrimentally siphon energy from the molecule, whereas collisions after laser excitation [which are the only important collisions at lower operating pressures (40 Torr)] are always of the latter detrimental variety. Since these detrimental collisions appear to severely affect the observed yield of only Freon 123d, and since they actually do not affect the laser–molecule interaction, a model which allows for energy quenching after laser excitation (which still has ϕ_{sat} as a parameter) is used to analyze the Freon 123d data; it is described in detail in Sec. V A. As is discussed in Appendix B, ϕ_{sat} is determined from data at only a specific gas mixture and therefore ϕ_{sat} will include the effect of the beneficial collisions.

1. 2,2-Dichloro-1,1,1-trifluoroethane photoproduct yield

The deuterium-bearing species in dissociation of 2,2-dichloro-1,1,1-trifluoroethane (Freon 123) is trifluoroethylene ($CF_2{=}CFD$). The trifluoroethylene photoproduct [$P(26)$, 10.65 μ] was monitored by GC as detailed in Sec. II C for neat CF_3CDCl_2, natural isotopic abundance Freon 123, and CF_3CDCl_2 mixed with various pressures of added CF_3CHCl_2. Because of the severe collisional quenching of larger molecules that have been

TABLE IV. Dissociation parameters of Freon 123 using 2 ns duration CO_2 laser pulses at $P(26)$, 10.65 μ.

Run no.	Photolysis pressure (Torr)	δ (%) CF_3CDCl_2	No. pulses	Energy (J)	Fluence[a] ϕ (J/cm^2)	Bulk yield[b]	Fractional yield[c] γ_D	η[d]	ϕ_{sat}[d]
1	1.00	98	1	0.82	60	4.89×10^{-3}	4.98×10^{-3}	5.34	11.2
2	5.00	3.28	25	0.42	31 ± 8	1.04×10^{-3}	9.61×10^{-4}	2.22	14.2
3	15.00	3.28	50	0.17	12.5 ± 3	6.04×10^{-5}	3.57×10^{-5}	0.944	13.7
4	30.00	0.0181[e]	15	0.60	44 ± 9	7.65×10^{-5}	4.99×10^{-4}	4.07	11.0

[a] Peak focal fluence on axis, determined from $2/\pi\omega_0^2$ times pulse energy.

[b] Obtained from GC analysis of photolysis products [Eq. (34)].

[c] Calculated from Eq. (33b) using $x = 1$ and $\beta = 100$.

[d] Peak focal fluence (assuming no absorption) is η times the saturation fluence; collision model described in the text (sec. V.A) is used to help obtain η.

[e] Natural isotopic abundance Freon 123.

excited above the decomposition energy after the laser pulse, a model which takes into account these collisions (Sec. V A) is applied to the data for Freon 123. The role of laser excitation in MPD is still determined by Eq. (35).

Equations (33) and (34) permit calculation of the fractional yield γ_D; $x = 1$ is used in Eq. (32), since one dissociated CF_3CDCl_2 molecule yields one $CF_2{=}CFD$ molecule. In addition, $\beta = 100$ was assumed in order to obtain γ_D; the exact choice of β [which is dependent on ϕ (see Fig. 16)] is not critical. The measured values of the fractional yield γ_D are summarized in Table IV for several photolysis mixtures. As shown in Table IV, the saturation fluence for Freon 123d is about 12 J/cm^2 for each run. The effect of severe collisional quenching in Freon 123d IR photolysis can also be discerned in Fig. 13, which depicts γ_D vs the total Freon 123 operating pressure without any absorption correction. Despite the lack of refined analysis, the evident substantial quenching of yield above 30–60 Torr in this figure truly illustrates the effect of collisions. (Note that Fig. 13 includes some data points not listed in Table IV.) Qualitatively different results were obtained in the MPD of the smaller molecules trifluoromethane and difluoromethane as reported in the following subsections.

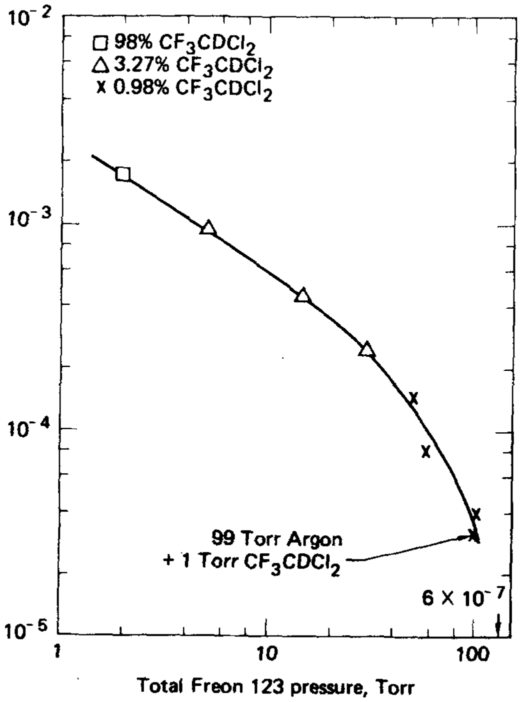

FIG. 13. The fractional yield per pulse γ_D for Freon 123 dissociation to yield trifluoroethylene using 2 ns duration CO_2 laser pulses at $P(26)$, 10.65 μ is shown as a function of total Freon 123 pressure. The fractional yield was calculated from Eq. (32) and is uncorrected for beam attenuation.

2. *Trifluoromethane photoproduct yield*

Trifluoromethane (CDF_3) was photolyzed using 2 ns duration CO_2 laser pulses at the $R(26)$, 10.21 μ CO_2 laser line. Photoproduct yields were determined by GC analysis of the tetrafluoroethylene product yields by the experimental procedure described in Sec. II C. In Eq. (32), $x = 2$ is used, since two trifluoromethane molecules are decomposed for each detected tetrafluoroethylene product. Since β is found to be very large ($\gtrsim 10\,000$) in CDF_3/CHF_3 photolysis (Sec. IV C and Refs. 10 and 11), the fractional yield γ_D is very insensitive to the exact value of β when the initial deuterium content exceeds about 1% [for $1/\beta \ll \delta$, Eq. (33b)]. A value of $\beta \approx 7000$ is assumed here; and the affect of a change in β is depicted in Fig. 14 and is discussed in Sec. IV C.

Data summarizing results for trifluoromethane are presented in Table V. Because of the great sensitivity of the dissociation probability $D(\phi)$ to fluence below saturation, all data in Table V are normalized to a constant fluence of 20 J/cm^2, as is indicated in the last column; some of this data is also presented in Figs. 14 and 15. In Fig. 14, the dissociation probability is plotted as a function of added argon pressure for an assumed fluence of 20 J/cm^2. For reference, the analogous curve for added CHF_3 (at $\phi = 20$ J/cm^2) is also shown. The dissociation yield with added CHF_3 is portrayed in Fig. 15 for irradiation by either 2 ns FWHM or 100 ns[9] FWHM pulses. The 2 ns duration pulse results were plotted for an assumed fluence of 27 J/cm^2 to permit proper comparison with the long pulse study which was performed with this fluence.

The first half of Table V indicates the influence of added argon; the dissociation probability of CDF_3 increases ~ six fold from the low pressure value to unity

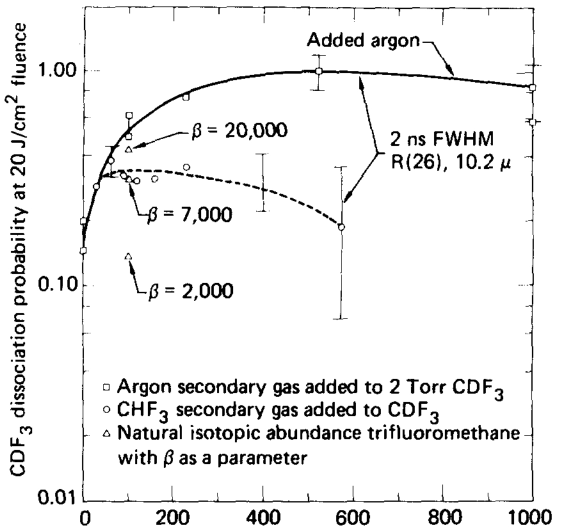

FIG. 14. The probability of CDF$_3$ dissociation by a 2 ns duration laser pulse at 20 J/cm^2 energy fluence [R(26), 10.21 μ line] is shown as a function of added secondary gas. The upper trace refers to added argon and the lower trace refers to added CHF$_3$.

dissociation probability near 1 atm of added argon. The consistency of the analysis procedure is indicated by Runs 3 and 4, both performed with 100 Torr added argon. The focal fluence used in Run 3 was 30% larger than in Run 4, and the resultant fractional yield was more than twice as high as is indicated in column 6; however, the resultant dissociation probabilities determined for $\phi = 20$ J/cm^2 for Runs 3 and 4 are comparable. D(20 J/cm^2) in Run 8 with 1030 Torr of added argon is slightly lower than in Runs 6 and 7 with 520 Torr added

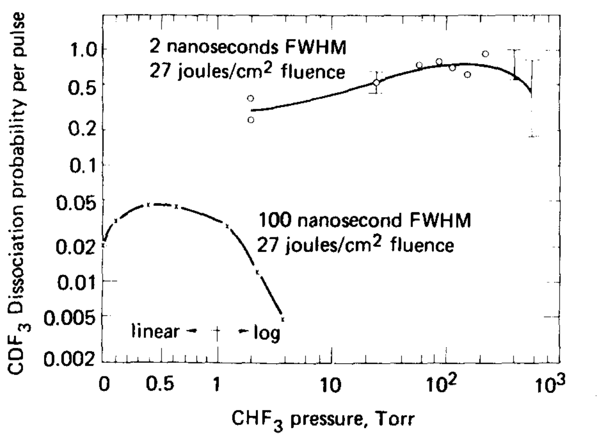

FIG. 15. The probability of CDF$_3$ dissociation by a CO$_2$ laser pulse at 27 J/cm^2 fluence [R(26), 10.21 μ] is shown as a function of added CHF$_3$ secondary gas. The upper trace refers to dissociation by a 2 ns duration laser pulse and the lower trace (Ref. 9) by a ~80 ns TEA laser pulse with a ~400 ns weak tail.

TABLE V. The influence of secondary gas pressure on the dissociation probability of CDF$_3$ using 2 ns duration CO$_2$ laser pulses at R(26), 10.21 μ.

Run no.	Secondary gas (Torr)	δ (%) CDF$_3$ [a]	$2E_i/\pi\omega_0^2$ (J/cm^2)[b]	Bulk yield[c]	Fractional yield per pulse[d] γ_D	η[e]	ϕ_{sat}^{f}	$D(20)$[g]
1	None	98.	32.5 ± 8	4.85×10^{-3}	2.19×10^{-4}	0.95	37.2	0.155
2	None	98.	30.7 ± 10	3.49×10^{-3}	1.42×10^{-4}	0.82	42.8	0.102
3	Argon-98	98.	25.9 ± 10	6.65×10^{-3}	2.93×10^{-4}	1.09	28.4	0.35
4	Argon-101	98.	18.3 ± 6	2.27×10^{-3}	1.30×10^{-4}	0.84	25.1	0.51
5	Argon-220	98.	20.3 ± 7	4.29×10^{-3}	2.13×10^{-4}	1.04	22.7	0.68
6	Argon-520	98.	26.3 ± 10	5.39×10^{-3}	6.87×10^{-4}	1.64	18.6 ± 0.5	1.0
7	Argon-520	98.	25.0 ± 9	12.35×10^{-3}	5.66×10^{-4}	1.51	19.0 ± 0.5	1.0
8	Argon-1030	98.	22.5 ± 7	5.79×10^{-3}	2.61×10^{-4}	1.17	21.7	0.78
9	Argon-120	98.	Unphotolyzed	$< 3\times10^{-5}$	...	...	...	...
10	None[h]	98.	27.3 ± 10[h]	2.31×10^{-3}	0.941×10^{-4}	0.72[h]	45.0[h]	0.088[h]
11	Argon-103.5[h]	98.	31.1[h]	10.52×10^{-3}	4.25×10^{-4}	1.24[h]	26.2[h]	0.44[h]
12	CHF$_3$-25.9	7.03	27.4 ± 9	3.54×10^{-4}	2.00×10^{-4}	0.93	33.6	0.21
13	CHF$_3$-60.6	3.14	26.6 ± 8	1.69×10^{-4}	2.39×10^{-4}	1.01	29.6	0.31
14	CHF$_3$-86.3	2.23	29.2 ± 6	1.50×10^{-4}	2.68×10^{-4}	1.07	29.1	0.33
15	CHF$_3$-100[i]	0.0155[i]	27.0	1.48×10^{-6}	2.34×10^{-4}	0.96	30.1[i]	0.29[i]
16	CHF$_3$-114.3	1.69	2.9 ± 0.8	$< 1\times10^{-6}$	$< 2.4\times10^{-6}$	< 0.2	> 14	...
17	CHF$_3$-114.6	1.70	26.3 ± 7	7.98×10^{-5}	1.87×10^{-4}	0.96	30.1	0.29
18	CHF$_3$-156.3	1.25	24.8 ± 10	4.17×10^{-5}	1.62×10^{-4}	0.94	32.1	0.24
19	CHF$_3$-230	0.860	20.8 ± 6	1.87×10^{-5}	1.07×10^{-4}	0.84	27.7	0.38
20	CHF$_3$-400	0.986	27.8 ± 7	2.86×10^{-5}	1.14×10^{-4}	0.86–0.92	30 ± 3	0.22–0.41[j]
21	CHF$_3$-570	1.06	25.6 ± 8	8.78×10^{-6}	3.27×10^{-5}	0.60–0.92	38 ± 10	0.07–0.35[j]

[a] δ is the percent of CDF$_3$ in total (CHF$_3$+CDF$_3$). In Runs 1–19 (except run 15) 2.0 Torr of CDF$_3$ was used.

[b] Peak focal fluence if no absorption were present, calculated from the average incident pulse energy E_i.

[c] Measured from GC yields, using Eq. (34) with $\chi = 7.94$.

[d] Calculated from Eq. (33b) using $\beta = 7000$. Only Run 15 is sensitive to the chosen β.

[e] η is the ratio of the actual fluence (including absorption) to the saturation fluence on axis at focus.

[f] Saturation fluence calculated from Eq. (B6). Fluence at which $D(\phi_{sat}) = 1.0$.

[g] Dissociation probability at constant 20 J/cm^2 fluence calculated using Eq. (35).

[h] Pulse duration is 12 ns.

[i] Natural isotopic abundance trifluoromethane with $\beta = 10\,000$ and $\delta = 150$ ppm. See Fig. 17 for effect of δ or β variations.

[j] Laser absorption in the cell was too severe in these cases to allow for accurate analysis.

TABLE VI. The influence of added CH_2F_2 on the dissociation probability of $CHDF_2$ using 2 ns duration CO_2 laser pulses at $P(14)$, 10.53 μ.

Run No.	CH_2F_2 (Torr)	δ (%) $CHDF_2$[a]	$2E_i/\pi\omega_0^2$ (J/cm^2)[b]	Bulk yield[c]	Fractional yield γ_D[d]	η[e]	ϕ_{sat}[f] (J/cm^2)	$D(20)$[g]
1	50.3[h]	3.70[i]	27.4 ± 5	2.94×10^{-4}	3.12×10^{-4}	1.09	26.2	0.44
2	101.1[h]	1.89[i]	29.3 ± 8	1.58×10^{-4}	6.50×10^{-4}	1.45	21.7	0.79
3	195.1[h]	1.00[i]	22.3 ± 5	5.91×10^{-5}	2.26×10^{-4}	0.995	24.0	0.58
4	200.0[h]	0.030[h]	28.2 ± 6	8.60×10^{-6}	4.85×10^{-4}	1.22[j]	24.2[j]	0.57[j]
5	438.1[h]	0.899[i]	22.1 ± 6	9.00×10^{-5}	3.80×10^{-4}	1.28	19.1	1.00

[a] δ is the percent $CHDF_2$ in total difluoromethane, including natural $CHDF_2$ in the added CH_2F_2 (see footnote h).

[b] Peak on-axis focal fluence if no absorption were present, calculated from the average incident pulse energy E_i. The indicated variation is one standard deviation.

[c] Calculated from GC yields using Eq. (34) with $\chi = 3.5$.

[d] Calculated from Eq. (33) using $\beta = 2500$ and $x = 2$.

[e] η is the ratio of the actual fluence (including absorption) to the saturation fluence on axis at focus.

[f] Saturation fluence calculated from Eq. (B6).

[g] Dissociation probability at constant 20 J/cm^3 fluence, calculated using Eq. (35).

[h] Natural isotopic abundance difluoromethane; 150 ppm deuterium corresponding to 0.03% $CHDF_2$ is assumed.

[i] In addition to the indicated pressure of $CHDF_2$ is an additional 0.24 Torr of CD_2F_2 (0.48 Torr CD_2F_2 for Run 5).

[j] $\beta = 2500$ assumed. See Fig. 18 for the effect of variation in δ and β.

argon. This may indicate the slow onset of yield quenching by argon.

The CDF_3 dissociation probability with added CHF_3 is tabulated in the second half of Table V, and the results are also visually portrayed in Fig. 15. The dependence of the CDF_3 dissociation yield with added CHF_3 is similar to that with added argon to about 50 Torr; it then seems to remain constant out to 200–300 Torr, and may fall slowly at high pressures. Excessive laser absorption within the cell limits the accuracy of the higher pressure ($\gtrsim 400$ Torr) data taken. For equal buffer pressures ϕ_{sat} is a little higher for added CHF_3 than for Ar; for example, for ~ 220 Torr of added buffer, for argon $\phi_{sat} \cong 23$ J/cm^2, while for CHF_3 it is $\cong 28$ J/cm^2. It is clear that with either secondary gas trifluoromethane-*d* is much more resistant to collisional quenching than is the ethane derivative (Freon 123-d).

Experiments 10 and 11 in Table V were performed using 12 ns duration pulses, rather than 2 ns pulses, for dissociation. No clear distinction is indicated from a comparison with Runs 1–4, performed with 2 ns duration pulses; both sets include runs performed for neat CDF_3 and CDF_3 with 100 Torr added argon. On the other hand, a very large effect was noted in going from 2 to 100 ns duration pulses as indicated in Fig. 15. It is clear from Fig. 15 that the yield increases by about an order of magnitude, and the maximum operating pressure increases by about 2 orders of magnitude, when the CO_2 laser pulse is shortened by about 2 orders of magnitude.

3. *Difluoromethane photoproduct yield*

Difluoromethane $CHDF_2$ was photolyzed using 2 ns duration CO_2 laser pulses at the $P(14)$, $\lambda = 10.532$ μ line. The sample of deuterated difluoromethane contained 32% $CHDF_2$, 64% CH_2F_2, and 4% CD_2F_2. The dominant photoproduct detected by flame ionization GC was monofluoroacetylene ($HC{\equiv}CF$). In calculating γ_D, the parameters $x = 2$ [refer to Eq. (17)] and $\beta = 2500$ (refer to Fig. 18) were employed.

In Table VI the dissociation probability of $CHDF_2$ is calculated, based on the experimentally determined dissociation yield, for 50–400 Torr of added CH_2F_2. The dissociation probability appears to slightly increase with higher CH_2F_2 pressure from its value at 50 Torr, but from 100–400 Torr of added CH_2F_2 the yield is approximately constant, within experimental scatter, and is characterized by $\phi_{sat} = 23 \pm 3$ J/cm^2. Runs (3) and (4) were performed with nearly the same total difluoromethane pressure but with different $CHDF_2$ partial pressures for the deuterium enrichment measurement described in the following subsection. Evidently, difluoromethane has a lower saturation fluence than trifluoromethane, since $\phi_{sat} = 23 \pm 3$ J/cm^2 is indicated in Table VI compared to $\phi_{sat} = 29 \pm 2$ J/cm^2 for trifluoromethane, with 50–400 Torr of the parent molecule as buffer.

C. Single-step deuterium enrichment factors

1. *Mass spectrometric analysis*

The single-step deuterium enrichment factor β in the trifluoroethylene photoproduct from Freon 123 photodissociation at 10.65 μ has previously been found to be very sensitive to fluence.[8] Low pressure (0.5 Torr) dissociation of Freon 123 with ~ 100 ns duration standard TEA CO_2 laser pulses resulted in single-step deuterium enrichment factors ranging from 30 near 100 J/cm^2 fluence to 1400 near 10 J/cm^2 fluence.[8] In the present study the influence of pressure on the single-step deuterium enrichment factor was measured for 2, 12, and 80 ns FWHM dissociating pulses at $P(26)$, 10.65 μ. These results are tabulated in Table VII, and show surprisingly little sensitivity to operating pressure. The data for this table were taken using the mode-locked CO_2 laser shown in Fig. 1 with a focused beam using a $f = 150$ cm f.l. lens. This focusing geometry resulted in a spot diameter of about $2\omega_0 = 1.8$ mm (1.1 times diffraction

TABLE VII. Freon 123 single-step deuterium enrichment β in trifluoroethylene phtooproduct.

Fill pressure (Torr)	Pulse duration FWHM (ns)	Pulse energy[a] E_i (mJ)	Calc. peak fluence[b] (J/cm^2)	#Pulses	Initial D/H	Final D/H	β[c]
3.06	2	220 ± 30	16	10	0.00424	4.2 ± 0.6	1000 ± 140
10.0	2	188 ± 35	14	10	0.00424	3.9 ± 0.8	900 ± 200
30.0	2	197 ± 80	15	10	0.00424	3.9 ± 0.3	730 ± 70
30.0	2	350 ± 28	26	15	0.000181[d]	0.30 ± 0.06	1600 ± 300
100.0	2	274 ± 34	17	20	0.00424	10 ± 3	2400 ± 700
100.2	2	318 ± 62	24	20	0.000181[d]	0.24 ± 0.01	1250 ± 100
1.002	12	197 ± 31	15	25	0.00463	3.15 ± 0.2	680 ± 40
3.06	12	193 ± 16	14	25	0.00463	3.76 ± 0.6	812 ± 130
10.11	12	182 ± 24	13	25	0.00463	3.83 ± 0.2	828 ± 50
30.1	12	181 ± 16	13	25	0.00463	4.22 ± 0.3	912 ± 60
30.4	12	183 ± 29	14	20	0.000181[d]	0.254 ± 0.03	1350 ± 200
60.2	12	208 ± 21	15	20	0.00463	4.14 ± 0.8	895 ± 170
100.2	12	183 ± 15	14	25	0.00463	No yield	···
0.369	80	523 ± 28	39	15	0.00463	0.74 ± 0.01	160 ± 2
1.002	80	525 ± 26	39	10	0.00463	0.96 ± 0.02	207 ± 4
3.08	80	427 ± 158	32	10	0.00463	1.27 ± 0.02	274 ± 6
10.38	80	503 ± 52	37	10	0.00463	1.24 ± 0.13	268 ± 30
30.0	80	525 ± 39	39	10	0.00463	1.05 ± 0.02	226 ± 3
0.305	80	551 ± 40	246[e]	10	0.00424	0.116 ± 0.03	39 ± 7
1.006	80	581 ± 25	259[e]	10	0.00463	0.176 ± 0.02	38 ± 5
3.00	80	558 ± 50	249[e]	10	0.00424	0.221 ± 0.01	51 ± 2
3.08	80	577 ± 42	257[e]	10	0.00424	0.151 ± 0.02	35 ± 5
10.0	80	565 ± 23	252[e]	10	0.00424	0.122 ± 0.01	29 ± 2
10.06	80	595 ± 14	265[e]	10	0.00463	0.124 ± 0.01	27 ± 2
22.8	80	568 ± 28	253[e]	10	0.00463	0.141 ± 0.01	31 ± 2
25.0	80	578 ± 34	258[e]	10	0.00424	0.152 ± 0.01	36 ± 2
50.0	80	547 ± 46	244[e]	10	0.00424	0.091 ± 0.01	21 ± 1

[a] Incident pulse energy; the indicated variation is one standard deviation.

[b] Peak on-axis focal fluence if no absorption were present, calculated from $2E_i/\pi\omega_0^2$.

[c] Single-step deuterium enrichment factor calculated using Eq. (1b).

[d] Natural isotopic abundance Freon 123 used.

[e] $f = 61$ cm focusing optics used.

limited, 1.2 cm diameter input beam) and a beam confocal parameter ($2z_R$) of about 50 cm. The indicated fluence in Table VII is the calculated peak focal fluence at the center of the Gaussian beam for an empty cell; this is exactly twice the average focal fluence calculated by dividing the beam input energy by $\pi\omega_0^2$ (ω_0 is the $1/e^2$ intensity beam waist). The single-step enrichment factor β in Table VII was calculated from Eq. (1b), and the D/H ratio was determined from the mass 64/63 ratio after subtracting contributions to each mass peak from background, carbon-13 contributions, and residual Freon 123, as discussed in Sec. II.

The quoted error in pulse energy listed in Table VII is the standard deviation of the measured energy per pulse. Typically, 10–25 pulses were used per enrichment measurement. The error in the final D/H ratio is not the intrinsic experimental accuracy, but rather the measurement accuracy, i.e., the variance in D/H ratio determined by 3–6 successive enrichment measurements on the same sample by the mass analyzer. Thus, the quoted error in the single-step deuterium enrichment factor β is an indication of relative precision between enrichment runs. Some of the data from Table VII is portrayed in Fig. 16 to facilitate visual comparison. Figure 16 clearly show the relative insensitivity of β to operating pressure. The drop in β in Fig. 16 that is observed for the data obtained with an 80 ns pulse duration is, in fact, due to the higher peak focal fluence (~ 37 J/cm^2) employed in this case compared to the more modest fluence (~ 15 J/cm^2) used for the 2 and 12 ns

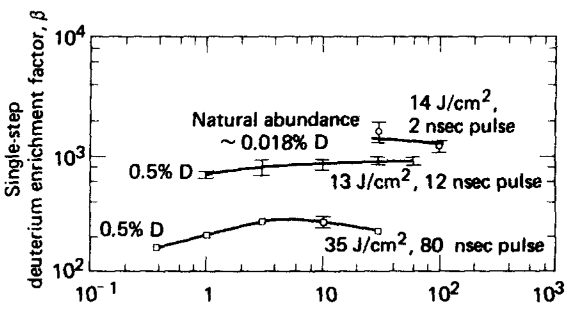

FIG. 16. The single-step deuterium enrichment factor in the trifluororethylene photoproduct from photolysis of Freon 123 at the $P(26)$, 10.65 μ CO_2 laser line is shown as a function of total Freon 123 pressure. The top curve refers to dissociation of natural isotopic abundance Freon 123 ($\delta \sim 0.018\%$) using 2 ns duration pulses; the middle and bottom curves refer to dissociation of Freon 123 containing 0.5% CF_3CDCl_2 using 12 and 80 ns pulse durations.

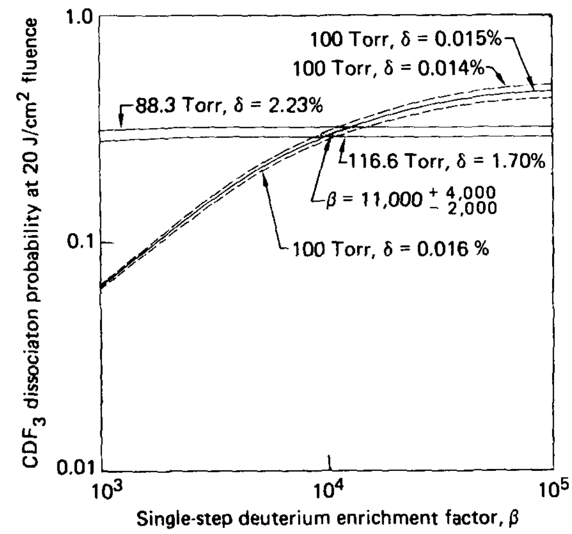

FIG. 17. The CDF_3 dissociation probability for 2 ns duration $R(26)$, 10.21 μ CO_2 laser pulses at 20 J/cm^2 fluence is displayed as a function of the assumed value of the single step deuterium enrichment factor β. The two nearly horizontal solid curves refer to the CDF_3 dissociation probability of 2 Torr CDF_3 buffered by 86.3 Torr of CHF_3 (upper curve) and buffered by 114.6 Torr CHF_3 (lower curve). The dotted curves bracket the CDF_3 dissociation probability based on dissociation of natural trifluoromethane ($\delta = 0.014\%–0.016\%$) at 100 Torr. The intersection of these curves near $\beta = 11\,000$ yields the most consistent value for β.

duration pulse studies (see Fig. 2 in Ref. 8). Table VII also clearly indicates the strong drop in enrichment to $\beta \approx 30$ at very high fluences near 250 J/cm^2. Deuterium enrichment at high pressure (≥ 100 Torr) was not achievable because no photoproduct was detectable. This is expected due to both collisional quenching and the loss of fluence due to beam attenuation by CF_3CHCl_2 (Sec. IV B).

2. Gas chromatographic analysis

A technique to determine the deuterium enrichment factor β indirectly from gas chromatographic analysis of the photoproduct is used to estimate β for trifluoromethane and difluoromethane. This technique was originally developed by Tuccio and Hartford[11] for isotope analysis in the trifluoromethane system, due to the difficulty in direct mass-spectrometric analysis of the HF/DF photoproduct. As described in Sec. II C, the accuracy of this technique for trifluoromethane analysis has previously been confirmed.[10] In the present study this indirect determination of deuterium enrichment factors is a by-product of the determination of dissociation probabilities, described in Sec. IV B. It is assumed that the dissociation probability is independent of δ for a given total pressure, when the initial concentration of the deuterated species δ is < 0.05. The dissociation probability is first measured by GC for δ near 1%; the dissociation probability thus determined is quite insensitive to the precise value of β, provided $\beta > 100$. Then an experiment is performed with a different δ (which in this experiment is natural deuterium isotopic abundance) at the same total pressure as before, and the value of β entering Eq. (33) is adjusted to yield the same dissociation probability (normalized to the same fluence) as obtained for δ near 1%.

Trifluoromethane. The single-step deuterium enrichment factor β was determined for trifluoromethane dissociation at 100 Torr using 2 ns CO_2 laser pulses at $R(26)$, 10.2 μ, utilizing Runs 14, 15, and 17 of Table V and is displayed in Fig. 17. Run 15, Table V at natural isotopic abundance was performed at 100 Torr; the trifluoromethane deuterium natural isotopic abundance was taken to be $\delta = 150$ ppm.[21] Since a run at 100 Torr was not performed with initially high deuterium content δ, Run 14 at 86.3 Torr and Run 17 at 114.6 Torr with $\delta \simeq 2\%$ were used instead; these exhibit nearly identical dissociation probabilities and consequently well bracket the value sought at 100 Torr. The curves in Fig. 17 intersect at a common dissociation probability of D(20 J/cm^2) $= 0.31 \pm 0.02$ for $\beta = 11\,000^{+4000}_{-2000}$. The uncertainty in the determined value of β stems from the uncertainty in dissociation probability and from the ± 10 ppm uncertainty in the deuterium isotopic abundance of natural trifluoromethane. This very high value of β measured near 100 Torr for 2 ns duration pulses is consistent with values of approximately 10 000 measured at low pressure using 100 ns duration pulses using the adjacent 10.2 μ, $R(28)$ CO_2 laser line.[10] Guided by the results of Ref. 10, β is expected to be even higher near 10.3 μ.

In the original paper describing use of GC analysis for determination of deuterium enrichment in the trifluoromethane system,[11] the loss of CF_2 radicals to processes other than recombination was taken into consideration according to the processes[11]

$$[CF_2] = \gamma_D[CDF_3] + \gamma_H[CHF_3] \; , \tag{40}$$

$$\frac{d[CF_2]}{dt} = -k_1[CF_2]^2 - k_2[CF_2] \; , \tag{41}$$

where Eq. (40) describes production by a single pulse of a concentration $[CF_2]$ of CF_2 radicals by dissociation of CDF_3 and CHF_3 with fractional yield γ_D and γ_H per pulse, respectively. The loss of CF_2 radicals is described by Eq. (41) and occurs at a rate $k_1[CF_2]$ due to recombination and at a rate k_2 due to other processes, such as reaction with C_2F_4, polymerization, walls reactions, etc. The ratio L of the rate of CF_2 loss to unknown mechanisms to the rate of total CF_2 loss is given by

$$L = \frac{k_2[CF_2]}{k_1[CF_2]^2 + k_2[CF_2]} = \frac{1}{1 + k^{-1}[CF_2]} \; , \tag{42}$$

where $k^{-1} = k_1/k_2$. The ratio L represents the fractional loss of CF_2 to mechanisms other than production of C_2F_4, and hence represents a possible error source in determination of the deuterium enrichment factor β from measurement of C_2F_4 photoproduct in trifluoromethane photolysis. Since $\beta \lesssim \gamma_D/\gamma_H$, Eq. (42) may be rewritten using Eq. (40):

$$L \cong \frac{1}{1 + k^{-1}\gamma_D(\delta + 1/\beta)[CHF_3]} \; . \tag{43}$$

The constant k was measured to have the value $(5.5 \pm 0.7) \times 10^{-8}$ Torr for experiments performed at 4 Torr of trifluoromethane.[11] Substituting this value of k and the measured values of γ_D and δ for Run 15 in Table V

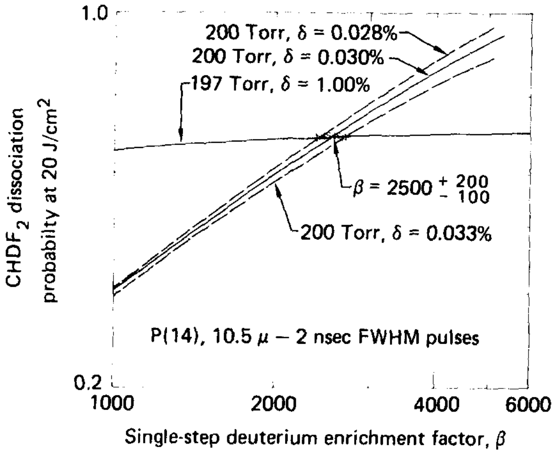

FIG. 18. The $CHDF_2$ dissociation probability for 2 ns duration $P(14)$, 10.54 μ CO_2 laser pulses at 20 J/cm^2 fluence is displayed as a function of the assumed value of the single-step enrichment factor β. The solid near-horizontal curve refers to the $CHDF_2$ dissociation probability buffered by 195 Torr CH_2F_2 and the dotted curves bracket dissociation of natural difluoromethane at 200 Torr ($\delta = 0.028\%-0.033\%$ $CHDF_2$). The curves intersect at the identical $CHDF_2$ dissociation probability $D(20\ J/cm^2) = 0.58$ for $\beta = 2500$.

at 100 Torr of CHF_3 at natural isotopic abundance, Eq. (43) indicates a calculated fractional loss of CF_2 radicals of $L \approx 0.014$. This small value of L stems from the high operating pressure of 100 Torr and the relatively large fractional yields γ_D of trifluoromethane dissociation in the present experiments. The calculated value of L for Runs 14 and 17 at higher initial CDF_3 concentrations is $L \approx 10^{-4}$. However, because of the reduced diffusion of CF_2 radicals stemming from the higher pressures and looser focus employed in the present experiments (compared to those in Ref. 11), k is expected to be smaller than the cited value; consequently, L is even smaller than the values calculated above. Thus, the determination of the single-step enrichment factor for trifluoromethane dissociation indicated in Fig. 17 is *not* significantly in error by the neglect of the fractional loss L of CF_2 radicals that fail to recombine to yield C_2F_4.

Difluoromethane. The difluoromethane single-step deuterium enrichment factor at $P(14)$, 10.5 μ was determined at 200 Torr using Runs 3 and 4 of Table VI. This data is displayed in Fig. 18, using Run 3 at 197 Torr containing $\delta = 1.0\%$ initial $CHDF_2$, and Run 4 at 200 Torr containing $\delta = 0.03\%$ initial $CHDF_2$ (natural isotopic abundance). The curves of Fig. 18 intersect at a common dissociation probability of $D(20\ J/cm^2) = 0.58$ for a single-step deuterium enrichment factor of $\beta = 2500^{+200}_{-100}$. This value of β obtainable using difluoromethane is intermediate between values of β near 1000 obtainable using Freon 123, and values of β near 10 000 obtainable using trifluoromethane. As described above, experimental uncertainties in the GC method for determination of β primarily stem from pulse to pulse variation in laser outpur energy, causing variation in dissociation yields, and hence calculated dissociation probabilities. A 20% uncertainty in dissociation probability is expected, and suggests a possible range of β for difluoromethane dissociation at 200 Torr of $1800 \leq \beta \leq 3500$.

V. DISCUSSION OF RESULTS

A. Features of the multiple-photon absorption process

In addition to the obvious implications to deuterium separation, the data presented in the previous section provides valuable insight into the nature of collision-free absorption and the effect of collisions in infrared multiple-photon absorption (MPA) and MPD. Of particular interest is the contrast between Freon 123d, which represents a medium to large molecule in the MPA sense, and trifluoromethane and difluoromethane, which are both small molecules.

There are two general features common to each of the plots of absorption coefficient α vs laser fluence for the monodeuterated molecules: (1) a low-fluence value of α which is approximately equal to that measured with an infrared spectrometer, and (2) a decrease in α with increasing fluence. The observed fluence dependence of α may be attributed to the effect of the gradual decrease in absorption cross section as the molecule climbs the vibrational ladder, in those molecules which interact with the laser. The decrease in α with increasing ϕ is much more drastic in neat CDF_3 (where α drops by a factor of 10 as ϕ is increased from very low fluences to 0.1 J/cm^2) than in neat Freon 123 (where the decrease is by less than a factor of 2 in the same fluence range). This different behavior can be traced to the differing fraction of molecules which interact with the laser in each case.

In neat, collision-free CDF_3 ($p < 10$ Torr with 2 ns pulses) only a small fraction (< 0.1) of available molecules interact with the laser. This "absorption bottleneck" was first noted by the authors in a previous study[9] using 100 ns FWHM laser pulses in which the photoproduct yield (as measured by GC) was found to be a steeply increasing function of added argon pressure. Subsequently, with the infrared fluorescence of the nascent MPD product $DF^{\dagger}$ being monitored, the authors observed a similar large increase (by a factor of > 25) in the dissociation probability of CDF_3.[20] In both experiments the argon buffer caused rotational transfer in CDF_3 during the laser pulse from states which do not interact with the laser (under the specific operating conditions) to those that do. This effect has also been noted in several other small molecules.[35] Evidently, the absorption coefficient data in Fig. 7 suggest similar behavior using 2 ns duration pulses. At fluences > 0.01 J/cm^2, the addition of argon induces beneficial state changing collisions during the laser pulse which allow a large fraction of all available molecules to undergo MPD; consequently, this lessens the severe decrease in α at higher fluences. Note that with the addition of ~ 1 atm of argon, α does not significantly decrease until $\phi > 0.1\ J/cm^2$. In addition, for $\phi > 0.1\ J/cm^2$, α is 10 times larger for the sample with the 1 atm of added buffer than for the pure unbuffered gas. A similar slow decline in α with increasing ϕ was observed in $CHDF_2$ with 1 atm of argon added. [No low pressure, neat $CHDF_2$ measurement of $\alpha(\phi)$ was performed.]

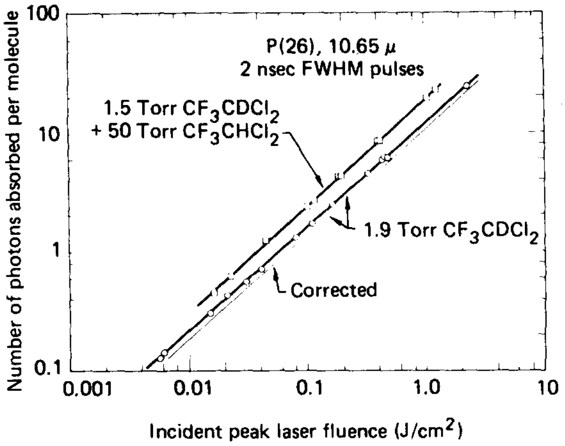

FIG. 19. The number of photons absorbed by CF_3CDCl_2 is displayed as a function of laser fluence for 2 ns duration pulses at $P(26)$, 10.65 μ. The curves refer to 1.5 Torr CF_3CDCl_2 buffered by 50 Torr CF_3CHCl_2 (upper curve) and 1.9 Torr neat CF_3CDCl_2 (lower two curves). The absorption cross sections were calculated using Beer's law (thick curves) and using Eq. (A9) (thin curve). The abscissa coordinate refers to the peak (local) fluence for the thick (thin) lines.

The very slow decrease in α with increasing ϕ in collision-free Freon 123d (Fig. 5) using 2 ns laser pulses is in marked contrast to the behavior of CDF_3. Apparently, in this large molecule an appreciable fraction of molecules ($\gtrsim 50\%$) interact with the laser without the need of state-changing collisions. The same interpretation can be inferred from the measurements by Black and Yablonovitch[36] of α in Freon 123d in which they employed both 0.5 and 100 ns duration pulses; Black and Yablonovitch observed only a ~45% increase in α (at 1 J/cm^2 fluence) when the peak laser intensity was increased by a factor of 200 (i.e., when the pulse width was decreased from 100 to 0.5 ns). The main effects of an increase in laser intensity at (low) constant fluence are to increase the probability of coherent multiquantum absorption and/or to increase ac Stark (power) broadening of transitions,[37] both of which tend to increase the number of molecules which interact with the laser in a manner similar to adding an inert buffer gas. Therefore, their observations also suggest that most Freon 123d molecules interact with the laser even in the collision-free regime. The effect of added CF_3CHCl_2 to CF_3CDCl_2 is discussed below.

The information provided by Figs. 5, 7, and 8 is replotted as the number of photons absorbed per molecule ($=\phi\alpha/\hbar\omega_{\rm laser}$) vs peak laser fluence in Figs. 19 and 20 for Freon 123d and trifluoromethane, respectively. The graphs for neat CDF_3, the CDF_3/Ar mixture and neat CF_3CDCl_2 corrected for aberrations from Beer's law behavior have also been plotted. (The identification of $\phi\alpha/\hbar\omega_{\rm laser}$ as the number of absorbed photons is exact only for the corrected curves.) For these corrected curves the abscissa actually refers to the laser fluence and not the peak fluence. Note that a break in slope in the CDF_3 + 780 Torr Ar curve occurs near 0.1 J/cm^2 and that the CDF_3 and CDF_3 + Ar plots are parallel for $\phi > 0.1$ J/cm^2.

If the CDF_3 + Ar plot is extended by continuing the linear behavior on the log–log plot to higher ϕ (though the slope will certainly decrease as CDF_3 begins to dissociate), it appears that an average of 33 quanta are absorbed per molecule at $\phi = 20$ J/cm^2. In the discussion of dissociation probability in Sec. IV B. 2 (Table V) the saturation fluence $\phi_{\rm sat}$ was determined to be about 20 J/cm^2 for CDF_3/(500–1000 Torr Ar) mixtures. To reach the activation energy for the MPD step of nascent DF elimination, the molecule requires ~69 kcal/mol or 25 CO_2 laser quanta. During the laser pulse a given CDF_3 molecule will continue to absorb quanta beyond the dissociation barrier until the dissociation rate equals the pumping rate.[38] Upon applying quantum RRK theory[39] to CDF_3 it appears that a molecule that absorbs three or more photons above the dissociation barrier will dissociate during the 2 ns long laser pulse. Since those that absorb fewer photons are subject to collisional deactivation after the laser pulse (for fluences near the saturation fluence), approximately 28 photons are required to dissociate each CDF_3 molecule. This is in surprisingly good agreement with the above calculation of about 33 quanta, based on the absorption coefficient. This latter calculated number is expected to slightly overestimate the number of absorbed photons, because the CDF_3/Ar (corrected) curve in Fig. 20 flattens near $\phi = 20$ J/cm^2. In addition, this calculation is very sensitive to the exact value of $\phi_{\rm sat}$ and to other experimental and calculation-related uncertainties (such as the straight line fit to the original data). The observed consistency between the absorption and dissociation probability measurements is most important.

A similar comparison can be made for neat Freon 123d. Based on the data in Table IV, $\phi_{\rm sat}$ for Freon 123d is approximately 12 J/cm^2. A straight-line extrapolation of the data in Fig. 19 suggests that approximately 90 photons/molecule are absorbed at $\phi = 12$ J/cm^2. Based on an ~78 kcal/mol activation energy for

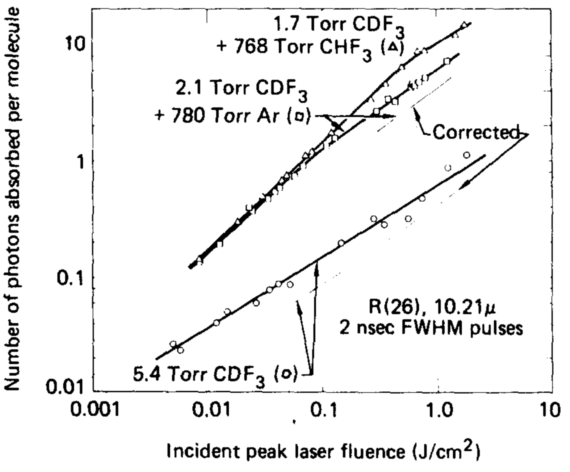

FIG. 20. The number of photons absorbed by CDF_3 is displayed as a function of laser fluence for 2 ns duration pulses at $R(26)$, 10.21 μ. The curves refer to CDF_3 buffered by 768 Torr CHF_3 (top curve), buffered by 780 Torr argon (two curves just below top), and to neat CDF_3 (lowest two curves). The thin lines refer to data corrected using Eq. (A9), and the thick lines to data calculated using Beer's law. See Fig. 19 caption for further details.

Cl atom elimination,[22] 29 quanta are required to reach the dissociation energy. The quantum RRK model suggests that ~ 35 additional quanta must be absorbed for decomposition during the laser pulse. In contrast, an RRKM treatment predicts that only ~ 16 additional photons need be absorbed,[23] suggesting that ~ 45 photons are required to decompose each molecule. Note that both calculations show that many more quanta are required to achieve dissociation during the laser pulse in the relatively large Freon 123d, *vis a vis* CDF_3. The estimate based on the absorption data is significantly higher than that calculated using either the RRKM or RRK result. Perhaps, $\phi_{sat} < 12$ J/cm^2, which would tend to decrease the estimate based on the absorption cross section. More importantly, the curve describing photon absorption in neat CF_3CDCl_2 in Fig. 19 must flatten for $\phi > 2$ J/cm^2, thereby making linear extrapolation less meaningful.

The effect of collisions on the MPA and MPD in Freon 123d, CDF_3 and $CHDF_2$ by noninert gases is quite important. Of particular interest in deuterium separation is the effect of collisions of the protonated species with the monodeuterated molecules. As is the case with inert buffers, molecular collision partners can help remove absorption bottlenecks. However, in contrast to rare gas collision partners, larger molecules can efficiently relax molecules which are excited in the quasicontinuum or in the continuum above the dissociation energy.[40] The consequences of these collisions are manifest in both the photon absorption and dissociation probability data.

In an earlier study[9] at low pressures (~ 1 Torr) with longer CO_2 laser pulses (FWHM $\simeq$ 100 ns), the addition of only 0.5 Torr CHF_3 was found to efficiently quench the dissociation yield in infrared photolysis of CDF_3. This data is reproduced in Fig. 15, alongside the present data taken with 2 ns duration pulses, which show that addition of CHF_3 ($\gtrsim$10 Torr) apparently enhances the dissociation probability due to the effect of state-changing collisions. No definite evidence of $CDF_3^\dagger$ quenching was found with up to 200 Torr of CHF_3 added. (Note that the data taken at > 200 Torr has a large experimental uncertainty.) This insensitivity to added CHF_3 stems from the rapid decomposition rate of CDF_3 excited a few quanta above the dissociation energy. Though collisions with CHF_3 may not prevent the dissociation of CDF_3 irradiated by the high intensity laser, $CDF_3^\dagger$–CHF_3 collisions may nonetheless siphon off a significant amount of energy from the CDF_3; this causes a larger depletion in the laser field and a greater net absorption of photons per dissociated CDF_3 molecule (i.e., a lower quantum efficiency) than would occur without these detrimental collisions. Figures 7, 8, and 20 suggest that *if* the addition of 1 atm Ar is sufficient to completely eliminate the absorption bottleneck, then the ~ 70% greater number of photons absorbed per CDF_3 with $\simeq$ 1 atm of CHF_3 added (instead of 1 atm Ar) is due to the $CDF_3^\dagger \rightarrow CHF_3$ siphoning. Note also that at comparable ϕ, the addition of CHF_3 apparently leads to a smaller increase in $D(20$ J/cm$^2)$ than adding an equal pressure of Ar—even though more photons are absorbed with CHF_3 than with Ar (Fig. 14). Further investigation is required to confirm this observation. The maximum permissible CHF_3 operating pressure in deuterium separation will most probably be determined by this siphoning effect and not by a decrease in yield which may occur at even higher CHF_3 pressures. The available experimental data suggests a satisfactory quantum yield for 100–200 Torr normal CHF_3/760 Torr Ar mixtures.

Though CF_3CDCl_2/CF_3CHCl_2 collisions apparently do not hurt the deuterium enrichment factor β (Fig. 16), they do have a quite detrimental effect on the dissociation probability. Collisions may be quite efficient in siphoning $CF_3CDCl_2^\dagger$ energy both during and after laser excitation. Since dissociation occurs during the laser pulses only if many (> 15) quanta are absorbed by the molecule above the activation energy, those molecules with somewhat less energy (which under collision-free conditions would normally dissociate after the laser pulse) may be collisionally quenched after the laser pulse and may never dissociate. At lower pressures of added CF_3CHCl_2 (< 40 Torr), only this type of collision is important, as is manifest in the raw data plotted in Fig. 13, which depict a rapid decline in yield vs CF_3CHCl_2 pressure. (Actually, the decline is a little less steep than shown because this data is uncorrected for the greater optical thickness of the medium at the higher pressures.)

The data in Table IV has been corrected for attenuation of the laser. Consistent values for ϕ_{sat} (11–14 J/cm^2) were obtained from Eq. (B6) (in Appendix B) for each data point only after the effects of collisions were removed by implementing the following model: The energy level spectrum of CF_3CDCl_2 is approximated by a molecular vibrational ladder with spacing of 580 cm^{-1} (= geometric mean of CF_3CDCl_2 modes) starting above the dissociation barrier; the dissociation rate of each level is evaluated by quantum RRK theory.[39] This rate is designated by Γ_n, for level n above the dissociation energy (level $n=0$). The state to state collisional quenching rate ($n \rightarrow n-1$) is Qp, where p is the pressure and Q is the quenching rate constant, which is *assumed* to be independent of n. Only $\Delta n = -1$ collisions are assumed, and because of the low experimental total pressures, only collisions after the laser pulse are considered. The simplifying assumption that after laser excitation only a single level n is populated is invoked—thereby ignoring the more realistic Poisson-like distribution of levels. The ensuing rate equations are straightforwardly solved; the solution then yields the fraction of initially excited molecules $F(n, p)$ that eventually dissociate ($0 \leq F \leq 1$):

$$F(n, p) = \sum_{m=0}^{n} \frac{\Gamma_m (Qp)^{n-m}}{\prod_{s=m}^{n} (\Gamma_s + Qp)} . \tag{44}$$

The measured fractional yield γ_D is set equal to the product of the normalized integration of the dissociation probability [Eq. (36) or (B6)] and $F(n, p)$; this consequently separates the effects of excitation (during the laser pulse) and quenching (after the pulse). Using this "poor man's" rate equation approach, a consistent set of values for ϕ_{sat} were obtained by assuming $n = 24$ ($\simeq$ 15 photons above the dissociation barrier) and that 1000

cm^{-1} are transferred during each gas kinetic collision. In quantum RRK theory $\Gamma_{24} \cong 37$ ns. In this analysis the values for n and Q ($= 1.9 \times 10^{-7}\, s^{-1}\, Torr^{-1}$) are by no means unique, as an increase in n with a suitable increase in Q predicts similar behavior.

Additional evidence of the importance of collisions in Freon 123d MPA is contributed by the absorption cross-section data. Figures 5 and 19 exhibit a 50% increase in net CF_3CDCl_2 absorption upon addition of 50 Torr Freon 123. (The contribution due to absorption by CF_3CHCl_2 has been subtracted.) Further analysis with data taken at various Freon 123 pressures and with other gases—such as argon added in addition to Freon 123—should help to differentiate between state-changing and the probably more important energy siphoning collisions.

Two other observations made in this study are noteworthy. First is the apparent increase in dissociation probability with increased laser intensity at constant fluence in CDF_3, shown in Fig. 15. The second point of interest is the apparent positive slope of the log–log plot of $\alpha(\phi)$ vs ϕ for CH_2F_2 in Fig. 12. Perhaps, part of the observed increase of α with ϕ may be spurious and attributable to difficulty in correcting this data for the contribution due to naturally occurring $CHDF_2$. The $CHDF_2$ contribution to α was determined from Fig. 11 where 1 atm of argon was used as a buffer, as opposed to the 1.3 atm of CH_2F_2 that buffers the naturally occurring $CHDF_2$ in Fig. 12. Based on the analogous data for CDF_3, α vs ϕ for $CHDF_2 + 1.3$ atm CH_2F_2 should be larger and flatter than with added argon, tending to lessen the upward slope in Fig. 12. Still, CH_2F_2 absorption data, uncorrected for the $CHDF_2$ contribution, shows some evidence of a positive slope for $P(12)$ and $P(18)$. A positive slope in α vs ϕ would suggest intensity-dependent coherent multiquanta absorption processes in CH_2F_2.

B. Applications to photochemical production of heavy water

In Sec. IV, the properties of three systems (Freon 123, trifluoromethane, and difluoromethane) were examined as part of the search for possible molecules for photochemical deuterium separation. Specifically, the optical selectivity in absorption, dissociation probability, and single-step enrichment factor were measured for MPA and MPD, using 2 ns duration pulses at operating pressures near 100 Torr. These data are now analyzed in light of fundamental photochemical requirements for viable deuterium separation to determine the relative and absolute merits of each molecule. These requirements include efficient utilization of photons, low makeup costs (i.e., low cost of replacement molecules destroyed by the photochemical enrichment step), and ease of recycle [i.e., the regeneration of the laser-depleted deuterium bearing working molecules by a chemical exchange process tied to water (or natural gas)[14,41]]. Many of the details of this assessment have been relegated to Appendix C.

The significance of the stated requirements may be understood by considering the main steps for a possible working process for photochemical deuterium separation; these are schematically portrayed in Fig. 21, for a 100 Mg D_2O/year deuterium separation plant using trifluoromethane as the working gas example. Figure 21 indicates a reaction chamber where nanosecond duration pulses from a CO_2 laser of about 1.5 MW average power interact with trifluoromethane at a pressure of a few hundred Torr, possibly with an added inert buffer. Dissociation of CDF_3 yields DF, which is removed from the trifluoromethane in a stripping tower. The deuterium-depleted CHF_3 is sent to an exchange tower where it picks up deuterium by a chemical exchange process tied to water; following this it is dried, and the gaseous CHF_3 is finally returned to the reaction chamber. Additional makeup

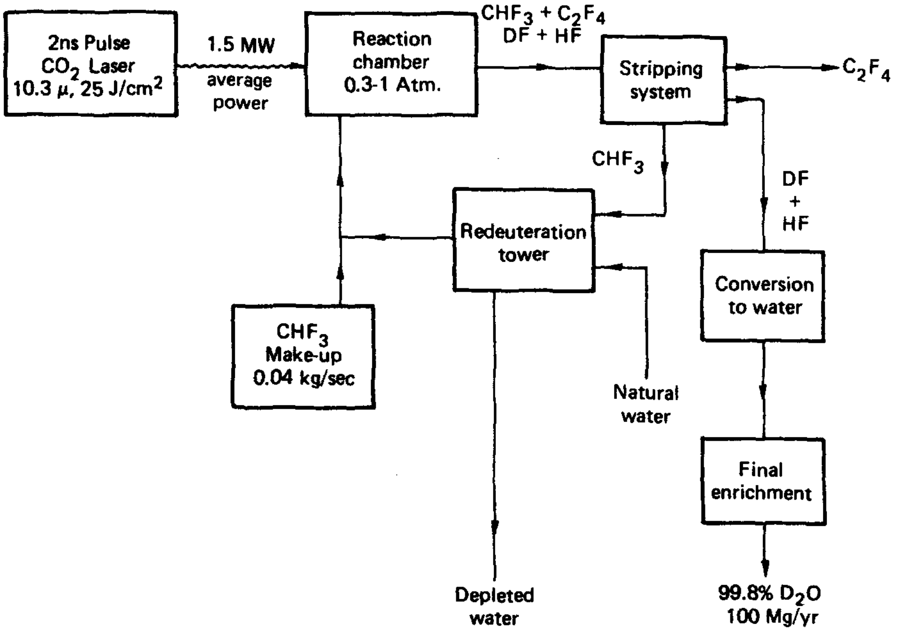

FIG. 21. The steps expected in heavy water production of CO_2 laser dissociation of trifluoromethane are schematically illustrated. Trifluoromethane gas containing CDF_3 enters a reaction cell at about 0.5 atm pressure for irradiation by a CO_2 laser pulse at 10.3 μ with an average fluence of ~ 25 J/cm^2 and pulse duration of ~ 2 ns. The CDF_3 molecules are selectively dissociated, yielding DF which is subsequently removed in the stripping tower. DF is converted to water for final purification to D_2O. The trifluoromethane depleted in deuterium undergoes redeuteration (in a process which is tied to water), and is returned to the reaction chamber along with makeup trifluoromethane.

TABLE VIII. Process comparison in deuterium separation.

Working molecule	Deuterium abundance δ^a	Fluence ϕ^b (J/cm^2)	η^c	λ	$S(\phi)^d$	$\epsilon_p(\phi)^e$	$E_D{}^f$ (keV)
Freon 123	0.018%	10	29+16	10.65 μ, $P(26)$	~40	0.007	36.9
Difluoromethane	0.030%	23	26+3	10.53 μ,$P(14)$	~350	0.095	1.77
Trifluoromethane	0.015%	25	25+3	10.21 μ,$R(26)$	~900^g	0.118	1.43^g
Hydrogen sulfide—GS—currently employed process							1.13^h

[a] Natural deuterium abundance of halocarbon in equilibrium with natural water.

[b] Energy fluence for which the dissociation probability is near 0.8 at 100 Torr (10 Torr for Freon 123) for 2 ns pulses.

[c] First number is #photons to reach the dissociation barrier. Sum is actual number absorbed for dissociation.

[d] Deuterium optical selectivity in absorption at the stated fluence. Estimated using Eq. (A9).

[e] Photon efficiency for absorption in the deuterated species, determined from Eq. (C3b).

[f] Total electrical energy required per separated deuteron, estimated from Eq. (C4b) using $\epsilon_l = 0.05$, $\epsilon_x = 0.9$, $\epsilon_c = 0.9$, and $\epsilon_d = 0.5$, see Appendix C.

[g] S(25 J/cm^2) is expected to be > 1000 for $\lambda = 10.3\ \mu$, and the effective S for two-frequency MPD experiments is also expected to be > 1000, leading to $E_D \lesssim 1$ keV for trifluoromethane.

[h] Equivalent electrical energy of the GS process based on *total* process requirements of 2.6 keV thermal energy and 0.26 keV electrical energy per separated deuterium,[14] assuming 33% conversion efficiency of thermal to electrical energy.

trifluoromethane is added to replace that destroyed during the photochemical separation step. The utilization of photons in the reaction chamber can be optimized by proper reactor design,[12] but the efficient absorption of photons by the deuterated species at a fluence permitting a near-unity dissociation probability is an essential requirement for good photon utilization, as is discussed in Appendix C.

The photon absorption efficiency ϵ_p is the fraction of all absorbed photons that are absorbed in the deuterium bearing species. ϵ_p is fluence dependent and is given by Eq. (C3b), which is derived in Appendix C, assuming no significant siphoning of energy from the deuterated to the protonated molecule:

$$\epsilon_p(\phi) \cong \left[1 + \frac{1}{\delta S(\phi)}\right]^{-1}, \quad \delta \ll 1 . \tag{45}$$

Equation (45) gives ϵ_p, where δ is the average deuterium content of the working gas and $S(\phi)$ is the optical isotopic selectivity in absorption, determined by the absorption cross-section ratio at the operating fluence ϕ. Since the deuterium-bearing compound absorption cross sections are strongly fluence dependent, ϵ_p will also depend on operating fluence, and will decrease with increasing fluence. The energy per separated deuteron E_D is simply the molecular dissociation energy (~ 3–4 eV) divided by all the process efficiencies. From Appendix C [Eq. (C4b)]

$$E_D(\phi) = \frac{\bar{n}hc\left[1 + \dfrac{1}{\delta S(\phi)}\right]}{\lambda\, \epsilon_l\, \epsilon_x\, \epsilon_c\, \epsilon_d}, \tag{46}$$

where ϵ_l is the "wall-plug" photon generation efficiency (laser efficiency), ϵ_x is the deuterium-bearing photoproduct extraction efficiency, ϵ_c is the reaction chamber photon absorption efficiency, ϵ_d is the dissociation efficiency averaged over the laser beam profile, c = speed of light, λ = laser wavelength, and $\bar{n}$ is the average number of photons the deuterated molecule requires to dissociate. Equations (45) and (46) permit relative comparison of the three candidate working molecules and allow an *estimate* of the energy required per separated deuteron for comparison to the existing GS process. These comparisons are made in Table VIII. The optical selectivity $S(\phi)$ in Table VIII has been determined for conditions of rather complete rotational hole filling, i.e., a total working gas pressure of several hundred Torr, at a fluence where the peak dissociation probability is approximately unity. $S(\phi)$ for the fluorinated methanes, under these conditions, has been summarized in Fig. 22.

In Table VIII the important number for comparison of the three candidate working molecules is the photon efficiency ϵ_p given in the second to last column. Freon 123 has an unacceptably low photon efficiency of less than 1%, while both difluoromethane and trifluoromethane have comparable photon efficiencies near 10%. Even though difluoromethane has a lower optical isotopic selectivity, the higher natural abundance of the $CHDF_2$ species compensates to make it equivalent to trifluoromethane.

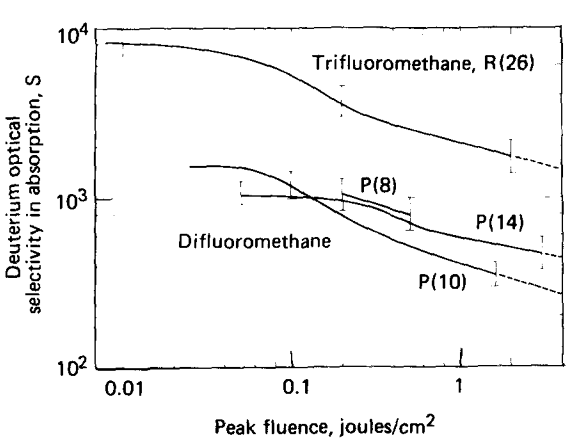

FIG. 22. The deuterium optical selectivity for absorption by 2 ns duration CO_2 laser pulses is displayed as a function of peak energy fluence. Data have been corrected using Eq. (A9) The curves refer to absorption in trifluoromethane at $R(26)$, 10.21 μ (top curve) and in difluoromethane near 10.5μ (lower three curves).

TABLE IX. Makeup requirements for photochemical deuterium separation.

		Makeup requirements	
Working molecule	β[a]	Moles[b]	kg[c]
Freon 123	1200	5.6	95
Difluoromethane	2500	2.33	13
Trifluoromethane	11000	1.58	12

[a] Single-step deuterium enrichment factor at 100 Torr from Sec. IV.C.

[b] #Moles working molecule destroyed per mole of separated deuterium atoms.

[c] Kilograms of working molecule destroyed per kilogram of produced D_2O, from Eq. (47) using $\epsilon_x = 0.9$ (Appendix C).

The last column in this table gives an estimate of the electrical energy required per separated deuteron for the optical separation stage *only* of a conceptual photochemical deuterium separation plant. For comparison purposes the total energy requirement of the currently used GS process is given in terms of equivalent electrical energy. Because of the uncertainities in the parameters entering Eq. (46) (see Appendix C), an exact comparison with the GS process is not yet feasible. However, Table VIII clearly shows that a process based on Freon 123 will use too much energy to even be seriously considered, but that a process based on either difluoromethane or trifluoromethane can be at least comparable to GS in energy requirements, and will use about 1 keV per separated deuteron in the photochemical separation stage. Naturally, energy costs associated with the rest of the deuterium separation plant, such as gas pumping and chemical exchange, would be added to the value in the last column in Table VIII. The only area where significant improvement appears feasible is photon efficiency ϵ_p, which is only 10% for the two methane derivatives. For example, a significant improvement in photon efficiency may be achieved by two frequency dissociation as discussed in Appendix C. In addition, S for CDF_3 can be increased by using $\lambda = 10.3\ \mu$.

The single-step enrichment factor β determines makeup costs in photochemical deuterium separation, i.e., the cost of replacement of all halocarbon working molecules destroyed in the isotopically selective dissociation step. This is given by the expression [Appendix C, Eq. (C10)]

$$\text{makeup}\left(\frac{\text{kg working molecule}}{\text{kg produced } D_2O}\right) = \frac{M}{10\,\epsilon_x}\left(1 + \frac{1}{\delta\beta}\right), \qquad (47)$$

where M is the molecular weight of the working molecule. Expression (47) gives the makeup in kilograms of working molecule per kilogram of produced D_2O. Table IX summarizes makeup requirements for the three candidate working molecules at initial deuterium concentration δ, based on the single-step enrichment factor β determined at 100 Torr (200 Torr for difluoromethane) using 2 ns dissociation pulses.

The third column in Table IX indicates the number of moles of working molecule destroyed per mole of separated deuterium. The last column is most relevant, and indicates the makeup mass in kilograms of working molecule per kilogram of D_2O product. (The cost of small halogenated alkanes often is independent of structure and proportional to bulk mass.[42]) The Freon 123 makeup cost alone[42] is comparable to the final value of the D_2O, whereas makeup costs would only contribute about 10% of final product value using either difluoromethane or trifluoromethane.[42] The lower deuterium enrichment factor β for difluoromethane is compensated by its lower molecular weight and higher natural $CHDF_2$ abundance δ, to make its makeup requirements equal to that for trifluoromethane.

Finally, the working molecule must undergo H/D chemical exchange to permit its recycling, as indicated in Fig. 21. Details on H/D chemical exchange rate constants available from the literature are summarized in Table X and discussed further in Appendix C. Freon 123 undergoes satisfactorily rapid H/D exchange in water catalyzed by added base (sodium hydroxide)[17]; however, it has been shown that its photochemical properties render it unsatisfactory. Very little data is available on chemical isotopic exchange for difluoromethane[43]; however, it is not expected to undergo base-catalyzed aqueous exchange at ambient temperature. Trifluoromethane undergoes slow aqueous-phase base-catalyzed exchange.[45(a)] Note that Table X indicates that hydrolysis occurs at a rate much slower than exchange,[45(a)] which is very fortunate. Ideally, hydrolysis should occur at a rate less than about 10^{-4} of the H/D exchange rate to avoid excessive replacement costs; this occurs for both Freon 123 and trifluoromethane. The trifluoromethane exchange pseudo-first-order rate constant of 5.4×10^{-4} s^{-1} at 70 °C in $pH = 14$ water[45(a)] is fairly small but comparable to the value of about $10^{-4}\ s^{-1}$ which appears to be required based on engineering studies.[45(b)] Possible alternatives are gas-phase (heterogeneous) isotopic exchange with natural gas over solid catalysts[21,45] or nonaqueous liquid-phase H/D exchange.[45(a),46] Table X indicates that considerably faster CHF_3 exchange will occur with liquid ammonia[16] (although CHF_3/NH_3 solvolysis is a problem[47]) or with methanol/dimethylsulfoxide (CH_3SOCH_3).[46] In this case the intermediate solvent itself undergoes H/D exchange with water to replenish deuterium.[48] In fact, recently the Chalk River Nuclear Laboratory has investigated deuterium isotopic exchange in trifluoromethane.[45a] Results of this investigation indicate that trifluoromethane isotopic exchange in water/dimethylsulfoxide mixtures catalyzed by NaOH is several orders of magnitude faster than in basic water.[45(a)] This is indicated in Table X and suggests that this system has a suitably fast deuterium exchange rate to be realistically considered for the redeuteration stage in a photochemical heavy water production plant.

VI. CONCLUSIONS

The dissociation yields, optical absorption cross sections, and single-step deuterium enrichment factors have been measured for 2,2-dichloro-1,1,1-trifluoroethane (Freon 123), difluoromethane, and trifluoromethane using CO_2 laser pulses as short as 2 ns in duration for MPD. Both the properties of absorption cross section vs fluence and yield vs secondary gas pressure of the fluorinated methanes and Freon 123 have been found to

TABLE X. Second-order rate constants of liquid-phase deuterium isotopic exchange.

Working molecule	Reference	Temp (°C)	Solvent system	Catalyst	Solvolysis rate constant[a] k_{hyd} (mol l^{-1} s^{-1})	Exchange rate constant[b] k_D (l mol^{-1} s^{-1})
CF_3CHCl_2	17	0	H_2O	NaOH	···	4.4×10^{-3}
CF_3CHCl_2	17	20	H_2O	NaOH	···	0.7×10^{-1}
CF_3CHCl_2	17	20	CH_3OH	CH_3ONa	1.5×10^{-9} [c]	1.4×10^{-2}
CHF_3	44	70	CH_3OH	CH_3ONa	···	1.1×10^{-5}
CHF_3	45a	70	D_2O	NaOD	$\sim 5\times 10^{-18}$	5.38×10^{-4}
CHF_3	45a	50	D_2O	NaOD	···	2.7×10^{-5}
CHF_3	43	100	1:1 D_2O/ CH_3COOD	K_2PtCl_4 [d]	···	1.8×10^{-6}
CHF_3	46	−30	ND_3	ND_2Na[e]	Slow[f]	4×10^{-5}
CHF_3	46	0	CH_3OD/ DMSO-d_6 [g]	CH_3ONa	···	7×10^{-2}
CHF_3	45a	49	51 mole % DMSO in H_2O	NaOH	···	2.6×10^{-1}
CH_2F_2	43	100	1:1 D_2O/ CH_3COOD	K_2PtCl_4 [d]	···	1.4×10^{-6}

[a] Rate of solvolysis (hydrolysis in aqueous media), i.e., rate of nonreversible reaction with the catalyst.

[b] Isotopic exchange rate of the working molecule in the indicated solvent; K_{obs} is assumed equal to the catalyst concentration times k_D in the range 0.001–2.5 mol/l; see Eq. (C16).

[c] Extrapolated from data at 55 °C, Ref. 17.

[d] Also contains $0.02M$ DCl.[43]

[e] Catalyst concentration not given,[46] assumed equal to 1 mol/l.

[f] Reaction rate with pure liquid ammonia is 2.3×10^{-7} s^{-1} at +25 °C (Ref. 47).

[g] Methanol/dimethylsulfoxide ratio not given[46]; this ratio is often 1:5 or 1:1.

conform to MPA–MPD standards for small and medium-large molecules, respectively.

The single-step deuterium enrichment factor is fairly independent of pressure for Freon 123 and attains a value of 1200 at 100 Torr; this is the maximum operating pressure because severe Freon 123 collisional quenching occurs above 50 Torr. The Freon 123 deuterium optical selectivity decreases from 100 at low fluence to about 50 at fluences where dissociation occurs. Overall, Freon 123 was determined to be *unsuitable* for potential large-scale photochemical production of heavy water. Difluoromethane has a single-step deuterium enrichment factor of 2500 at 200 Torr at $P(14)$, 10.5 μ, as indirectly determined from gas chromatographic analysis. Difluoromethane $CHDF_2$ has a deuterium optical selectivity greater than 1000 at low fluence [$P(8)$–$P(14)$ CO_2 laser lines, 10.5 μ] which decreases to about 350 at near-unity yield dissociation fluences. In addition, $CHDF_2$ exhibits dissociation yield saturation near 20–25 J/cm^2 fluence, and exhibits very little collisional quenching to 400 Torr, which was the highest pressure employed because of plasma breakdown. Trifluoromethane has the highest single-step deuterium enrichment factor of the three examined molecules; β is approximately 11 000 at 100 Torr as determined by gas chromatography with $\lambda = 10.2$ μ; much higher values of β are anticipated near 10.3 μ. Trifluoromethane CDF_3 exhibits photodissociation yield saturation near 30 J/cm^2, and also shows very little collisional quenching; photodissociation yield significantly decreases only above 500 Torr. The low pressure, neat CDF_3 absorption cross section falls very rapidly with increasing fluence, due to the decrease in cross section at higher vibrational levels and the small fraction of CDF_3 molecules participating in MPA. Addition of 1 atm of argon buffer gas permits effective rotational hole filling during a 2 ns duration laser pulse and results in a tenfold increase in the CDF_3 absorption coefficient at fluences above 0.1 J/cm^2. CHF_3 is a slightly more efficient collision partner (in regard to net medium absorption) as compared to argon at fluences above 0.1 J/cm^2. The deuterium optical selectivity of CDF_3 for absorption of 2 ns pulses at $R(26)$, 10.2 μ is 8000 below 0.01 J/cm^2, and decreases with increasing fluence to about 2000 at 2 J/cm^2. Overall, both difluoromethane and trifluoromethane exhibit satisfactory photochemical performance for possible large-scale production of heavy water by nanosecond-duration CO_2 lasers. In particular, there is great promise for a sucessful deuterium separation process specifically based on the MPD of trifluoromethane because of the available favorable techniques for deuterium replenishment.

ACKNOWLEDGMENTS

The authors wish to thank Ken Woodall for conveying his results of the measurement of the D/H ratio in normal trifluoromethane, Douglas Krajnovich for communicating to us the findings on molecular beam MPD and RRKM analyses of Freon 123, and Jerry Black and Eli Yablonovitch for conveying their results and for useful discussions on multiple-photon absorption in Freon 123. The authors also acknowledge the valuable discussions with Don Smith, Alistair Miller, Allan Symons, and John Rolston of the Chalk River Nuclear Laboratories regarding considerations important in the exchange step of a photochemical heavy water plant. In addition, the authors gratefully acknowledge financial assistance from the U.S. Department of Energy-Advanced Isotope Separation Branch.

APPENDIX A

The absorption coefficient and optical selectivity data presented in Sec. IV A were derived by measuring the transmission of an unfocused laser pulse through a medium of absorber pressure p and length l. The reported "uncorrected" results were obtained using a Beer's law formulation

$$\alpha = -\frac{1}{pl}\ln\left(\frac{\phi_{\rm out}}{\phi_{\rm in}}\right) , \qquad \text{(A1)}$$

where $\phi_{\rm in}$ and $\phi_{\rm out}$ are the laser fluence at the entrance and exit windows, respectively. Since in multiple-photon absorption α is a monotonically decreasing function of the fluence ϕ, the actual absorption coefficient at the peak fluence is lower than that determined from Eq. (A1) for two reasons. First, Eq. (A1) is an improper integration of the correct differential form when $\alpha = \alpha(\phi)$:

$$\frac{d\phi}{\phi} = -\alpha(\phi)p\,dz \qquad \text{(A2)}$$

(z is the coordinate along the direction of propagation), and secondly, the laser is more strongly absorbed in the wings of the transverse profile than in the center. These two corrections are considered sequentially.

A power law dependence for $\alpha(\phi)$ is assumed[49]:

$$\alpha(\phi) = \frac{A}{\phi^{\rho}} \quad (0 \le \rho < 1) \ . \qquad \text{(A3)}$$

After substituting Eq. (A3) into Eq. (A2) the latter can be integrated over the cell length l to yield

$$\phi^{\rho}_{\rm out} - \phi^{\rho}_{\rm in} = -\rho A p l \ . \qquad \text{(A4)}$$

Using the value for A determined from Eq. (A4), $\alpha(\phi)$ is obtained:

$$\alpha(\phi) = \frac{1}{\rho pl}\left(\frac{\phi^{\rho}_{\rm in} - \phi^{\rho}_{\rm out}}{\phi^{\rho}}\right) \ . \qquad \text{(A5)}$$

For the CDF_3 transmission experiments $\alpha(\phi)$ determined from Eq. (A5) was typically ~ 12% lower than α determined from Beer's law [Eq. (A1)]. ρ was found to range from 0.12 to 0.35 in these experiments.

This first ("longitudinal") correction would be sufficient for the analysis if the laser had a rectangular transverse profile. Since this is not the case, and since $d\alpha/d\phi < 0$, a further correction for the variation in absorption across the transverse laser profile must be considered. Kolodner *et al.*[28] have shown that for any additive function $f(\phi)$ of laser fluence (or intensity) which has been experimentally (or otherwise) averaged over the transverse Gaussian laser profile to yield $f_g(\phi)$ [where ϕ is the peak (central) fluence], $f(\phi)$ can be easily recovered by the relation

$$f(\phi) = f_g(\phi)\,\frac{d\ln f_g(\phi)}{d\ln\phi} \ . \qquad \text{(A6)}$$

For the additive property of transmittance $T(\phi) = \phi_{\rm in}\exp[-\alpha(\phi)pl]$, Eq. (A6) reduces to

$$\alpha(\phi) = \alpha_g(\phi) - \frac{1}{pl}\ln\left(1 - pl\phi\,\frac{d\alpha_g}{d\phi}\right) , \qquad \text{(A7)}$$

where $\alpha_g(\phi)$ is averaged over the Gaussian profile. If $pl\phi(d\alpha_g/d\phi) \ll 1$, as is true for the experiments reported in this paper, then

$$\alpha(\phi) \cong \alpha_g(\phi) + \phi\,\frac{d\alpha_g}{d\phi} \ . \qquad \text{(A8)}$$

This amounts to a necessary ~ 24% decrease in α from the uncorrected Beer's law α for the CDF_3 + 780 Torr argon case.

These two contributions are complementary. The first contribution modifies the treatment of the absorption of a plane wave along the direction of propagation; while the second effect corrects the data for the transverse Gaussian profile. In fact, due to this latter correction an initially Gaussian beam evolves into a decidedly non-Gaussian profile, an effect which is presently ignored. Though in an exact treatment both corrections should be considered together during propagation, when these corrections are employed in this analysis the transverse correction is applied to the data which has already been corrected for propagation effects; this slightly overestimates the overall correction. Nonetheless, applying Eq. (A8) to Eq. (A5) [in which $\alpha(\phi)$ is actually $\alpha_g(\phi)$ in the latter equation] yields

$$\alpha(\phi) = \left[\left(\frac{1-\rho}{\rho pl}\right)(\phi^{\rho}_{\rm in} - \phi^{\rho}_{\rm out})\right]\frac{1}{\phi^{\rho}} , \quad \rho \ne 0 , \qquad \text{(A9)}$$

$$= -\frac{1}{pl}\ln\left(\frac{\phi_{\rm out}}{\phi_{\rm in}}\right) , \quad \rho = 0 \text{ (Beer's law)} , \qquad \text{(A10)}$$

where the term in the bracket is the final value for A [Eq. (A3)], and ϕ is the local, and not necessarily the peak, fluence.

APPENDIX B

Expressions (37) and (39) in the text were obtained from Ref. 34 and assumed a power-law fluence dependent dissociation probability and an optically thin sample. That reference also gave a first order correction to these relations that allows for small amounts of absorption (< 15%) during the single pass of the laser through the reaction cell. This Appendix extends this correction to second order to more correctly handle the data obtained in the reported experiments, and also describes other procedures used in the analysis of the MPD yield data.

A general power law dependence is assumed for the dissociation probability D:

$$D(\phi, \lambda) = \bar{p}\left(\frac{\phi}{\phi_{\rm sat}}\right)^m , \quad \phi \le \phi_{\rm sat} , \qquad \text{(B1a)}$$

$$= \bar{p} , \quad \phi > \phi_{\rm sat} , \qquad \text{(B1b)}$$

where m is an integer and $0 < \bar{p} \le 1$. The radial dependence of the Gaussian beam is given by

$$\phi(r, z) = \phi(0, z)\exp[-2r^2/\omega^2(z)] , \qquad \text{(B2)}$$

and

$$\omega^2(z) = \omega_0^2\left(1 + \frac{z^2}{z_R^2}\right) , \qquad \text{(B3)}$$

where r and z are measured from the center of the cell (which is the focus), ω_0 is the beam radius at the focus ($z=0$), and z_R is the Rayleigh range ($z_R=\pi\omega_0^2/\lambda$). The Gaussian beam used in these experiments was measured to be 1.1 times diffraction limited, yielding a beam radius ω_0 at the focus equal to

$$\omega_0=1.1\frac{f\lambda}{\pi a}=87.54\lambda \text{ (cm)} , \tag{B4}$$

where f is the focal length of the lens, a is the input beam radius at the $1/e^2$ intensity point, and the rightmost expression is evaluated using the experimental conditions of $f=150$ cm and $a=0.6$ cm. The Rayleigh range in the yield experiments was about 25 cm, which is shorter than 59 cm, which is half the length of the photolysis cell.

In Sec. IV B, m was set equal to 3 on the basis of prior experimental evidence. In addition, the parameter $\bar{p}$ was assumed to equal 1. In many cases $\bar{p}$ may be less than 1 to account for MPD interaction with only a small subset of all molecules. For $\eta<1$, this parameter may be formally incorporated into ϕ_{sat}. In CDF_3 it has been found[9] that for a specific gas mixture $D(\phi,\lambda)$ eventually approaches unity at very high fluences, and therefore $\bar{p}$ may be set equal to 1—if ϕ_{sat} is determined for only that particular gas mixture. Consequently, the MPD dynamical and the pressure effects are characterized by variations in ϕ_{sat}.

The longitudinal dependence of the laser energy $E(z)$ is taken to be a second-order expansion of Beer's law:

$$E(z)=E\left\{1-\alpha N(z+l/2)+\frac{[\alpha N(z+l/2)]^2}{2}\right\} , \tag{B5}$$

where E is the energy at the input window ($z=-l/2$), α is the absorption coefficient, N is the density of absorbing species, and l is the cell length. For $\alpha=0$, $\phi(0,z)=2E/\pi\omega^2(z)$. The range of validity of Eq. (B5) is discussed below.

Inserting Eq. (B1) into Eq. (36) and using the techniques described in Ref. 34, the following expression is obtained for V_{eff}, which is the effective fractional dissociation volume, and is also equivalent to $V\gamma_D$ (or $V\gamma_H$) as defined in Sec. IV B: For $m\geq 2$,

$$V_{\text{eff}}=V^{+}_{\text{eff}}(2)+V^{-}_{\text{eff}}(2)+V_{\text{eff}}(1)+V_{\text{eff}}(0) , \tag{B6}$$

where

$$V^{\pm}_{\text{eff}}(2)=\frac{\pi\omega_0^2 z_R\bar{p}}{2}\left\{\frac{4m+3}{3m}\sqrt{(\eta-1)^{\pm}}+\frac{2m+3}{9m}[(\eta-1)^{\pm}]^{3/2} -\tfrac{4}{3}\arctan\sqrt{(\eta-1)^{\pm}}+\frac{\eta^m}{m}Af(x,m)\Big|_{x=\sqrt{(\eta-1)^{\pm}}}^{l/2z_R}\right\} , \tag{B7}$$

$$V_{\text{eff}}(1)=\frac{\pi\omega_0^2 z_R^2\bar{p}B}{4m(2-m)}\eta^m\frac{1}{(1+x^2)^{m-2}}\Big|_{\sqrt{(\eta-1)^{+}}}^{\sqrt{(\eta-1)^{-}}} \quad (m\geq 3) , \tag{B8a}$$

$$=\frac{\pi\omega_0^2 z_R^2\bar{p}B}{8}\eta^2\ln(1+x^2)\Big|_{\sqrt{(\eta-1)^{+}}}^{\sqrt{(\eta-1)^{-}}} \quad (m=2) , \tag{B8b}$$

$$V_{\text{eff}}(0)=\frac{\pi\omega_0^2 z_R^3\bar{p}C}{m}\eta^m[f(x,m-1)-f(x,m)]\Big|_{\sqrt{(\eta-1)}}^{l/2z_R} , \tag{B9}$$

with

$$f(x,m)=\frac{x}{2m-3}\sum_{k=1}^{m-2}\frac{1}{2^k}\frac{(2m-3)!!}{(2m-2k-3)!!}\frac{(m-k-2)!}{(m-2)!}\times\frac{1}{(1+x^2)^{m-k-1}}+\frac{(2m-5)!!}{2^{m-2}(m-2)!}\arctan x \quad (m\geq 2) , \tag{B10a}$$

$$f(x,1)=x , \tag{B10b}$$

$$\begin{aligned}\sqrt{(\eta-1)}&=0 , && \text{if } \eta<1 ,\\ &=l/2z_R , && \text{if } \eta>1+\left(\frac{l}{2z_R}\right)^2\end{aligned} \tag{B11}$$

or as determined from η otherwise,

$$\sqrt{(\eta-1)^{\pm}}=\sqrt{(\eta-1)+(\tfrac{3}{2}\eta-1)\frac{\eta z_R^2\alpha^2N^2}{2}+\eta\left(\frac{-\alpha Nl}{2}+\frac{\alpha^2N^2l^2}{8}\right)\pm\frac{\eta z_R}{2}\left(-\alpha N+\frac{\alpha^2N^2l}{2}\right)} \tag{B12}$$

if this is $<l/2z_R$ and if the term in $\sqrt{\ }$ is >0; however, it $=0$ if term in $\sqrt{\ }<0$, or it $=l/2z_R$ if $\sqrt{(\eta-1)^{\pm}}$ calculates to $>l/2z_R$,

$$A=1-\frac{\alpha mNl}{2}+\frac{\alpha^2m^2N^2l^2}{8} , \tag{B13a}$$

$$B=-\alpha mN+\frac{\alpha^2m^2N^2l}{2} , \tag{B13b}$$

$$C=\frac{\alpha^2m^2N^2}{2} . \tag{B13c}$$

Equation (B6) is fully corrected for the second order absorption correction that can be used for $m\alpha Nl\ll 1$, and was employed to analyze the yield data presented in Sec. IV B. It is important to note that the result is valid only if Eq. (B5) is a suitable representation of $E(z)$. One obvious limitation of Eq. (B5) is the actual optical thickness of the medium. A more important restriction stems from the fact that the multiple photon absorption coefficient α decreases with increasing fluence, as is clear from the data presented in Sec. IV A. In weakly focused beams in optically thin media this does not affect the results. However, in more tightly focused or in optically thicker media there are important modifications to $E(z)$, such as (1) a more complicated form for $E(z)$ due to both the focusing geometry and the non-Beer's law behavior of the transmitted fluence, and (2) allowance for distortions in the Gaussian beam propagation formula [Eq. (B3)] since the wings absorb radiation more strongly than do the central regions.[28] These qualifications slightly affect the data analysis in some of the experimental runs. The value of the absorption coefficient that is utilized in this analysis is that at half the peak focal fluence, which is determined from the data in Sec. IV A.

The influence of pulse-to-pulse variations in laser fluence on data analysis was also considered in the application of Eq. (B6). Since at fluences below saturation the yield increases as the cube of the fluence, inserting the pulse-averaged fluence into this equation tends to determine a falsely low value for ϕ_{sat}. This was remedied by suitably weighting the fluence by a Gaussian distribution of pulse fluences defined by the average fluence and standard deviation for each run, as listed in Tables IV–VI. For cases in which $\eta<1$, a ϕ^3 weighting factor was used, whereas for $\eta > 1$ a ϕ^2 factor was used to compensate for saturation effects. This weighted fluence was the actual fluence used in Eq. (B6).

APPENDIX C

The results of the measurements on optical absorption cross sections and single-step deuterium enrichment factors are now applied to the detailed comparison of Freon 123, trifluoromethane, and difluoromethane for potential application in large-scale photochemical production of heavy water. The measurements permit calculation of the photon utilization efficiency and the makeup requirements, as discussed below. In addition, the requirement of isotopic chemical exchange to replenish the deuterium in the working molecule is discussed.

Efficient utilization of photons in deuterium separation

The efficient use of photons is directly related to high "absorption selectivity" and is not directly correlated with a high single-step enrichment factor which is itself related to "dissociation selectivity." To illustrate this point, consider a situation where the fluence permits an average of 30 photons to be absorbed in each deuterium-bearing molecule and 1 photon absorbed on the average in each normal molecule (for an optical selectivity of 30). In this situation the deuterium bearing molecule can have a near-unity dissociation yield, but an average absorption of only one photon may lead to essentially zero dissociation in the protonated molecule. The dissociation selectivity, or β, will be very high, yet the large concentration of normal molecules, each absorbing one photon, will lead to extremely poor photon utilization. If the above example refers to deuterium separation at natural abundance, the ratio of photons used for dissociation to total absorbed photons would be about $30/6000 = 0.005$, assuming a 6000 to 1 ratio of H/D-bearing molecules. This example is very close to the actual situation for Freon 123.

The photon absorption efficiency at a given fluence $\epsilon_p(\phi)$ may be expressed as the ratio of photons absorbed in the deuterium bearing molecule to total absorbed photons, or

$$\epsilon_p(\phi) = \frac{N_D\sigma_D(\phi)}{N_H\sigma_H(\phi) + N_D\sigma_D(\phi)} = \left[1 + \frac{N_H/N_D}{\sigma_D(\phi)/\sigma_H(\phi)}\right]^{-1} , \tag{C1}$$

where N_D and N_H are the molecular densities of deuterium- and non-deuterium-bearing molecules, respectively, and $\sigma_D(\phi)$ and $\sigma_H(\phi)$ are the absorption cross sections, respectively of the monodeuterium- and non-deuterium-bearing molecules at the desired dissociation fluence and wavelength. Defining the isotopic selectivity in absorption $S(\phi)$ at a given fluence by

$$S(\phi) \equiv \frac{\sigma_D(\phi)}{\sigma_H(\phi)} = \frac{\alpha_D(\phi)}{\alpha_H(\phi)} , \tag{C2}$$

Eq. (C1) is rewritten, using the initial deuterium fraction δ [Eq. (25)] to yield

$$\epsilon_p(\phi) = \left[1 + \frac{1-\delta}{\delta S(\phi)}\right]^{-1} , \tag{C3a}$$

$$\cong \left[1 + \frac{1}{\delta S(\phi)}\right]^{-1} , \quad \delta \ll 1 . \tag{C3b}$$

Using the data of Sec. IV A, the deuterium absorption selectivity S was determined for trifluoromethane, difluoromethane, and 2, 2-dichloro-1, 1, 1-trifluoroethane, and is displayed in Fig. 22 as a function of fluence for difluoromethane and trifluoromethane. The data in Fig. 22 have been corrected for the fluence dependence of the absorption coefficient, as well as for the Gaussian beam profile, according to expression (A9) in Appendix A. These corrected values for the optical selectivity are lower than the uncorrected values obtained using Beer's law and must be employed in this analysis.

The photon absorption efficiencies ϵ_p for Freon 123, trifluoromethane, and difluoromethane are given in Table VIII in the text for a fluence of 10–25 J/cm^2. Approximate values have been estimated using Eq. (A9) for extrapolation to fluences at which the dissociation probability is about 0.8 for each molecule. The values of ϵ_p in this table are simply the percent photon absorption in the deuterium-bearing molecule at natural deuterium isotopic abundance.

Table VIII indicates that the Freon 123 photon absorption efficiency is only about 1% for separation of natural isotopic abundance deuterium. Both difluoromethane and trifluoromethane have comparable photon absorption efficiencies of about 10% [$\epsilon_p(\phi)$ for CDF_3 will be even higher for $\lambda \cong 10.3\ \mu$]. The calculated photon absorption efficiencies of Table VIII along with the measured dissociation probabilities given in Tables IV–VI now permit calculation of the photon utilization efficiency, and hence the net (electrical) energy required per separated deuteron.

The energy required per separated deuteron E_D is simply the energy required for dissociation (~ 3 eV) divided by the various efficiencies: photon production (laser efficiency) ϵ_l; molecular photon absorption ϵ_p; reaction chamber absorption efficiency ϵ_c; dissociation efficiency ϵ_d; and photoproduct extraction efficiency ϵ_x:

$$E_D(\phi) = \frac{\bar{n}hc}{\lambda\epsilon_l\,\epsilon_p\,\epsilon_x\,\epsilon_c\,\epsilon_d} , \tag{C4a}$$

$$= \frac{\bar{n}hc\left[1 + \frac{1}{\delta S(\phi)}\right]}{\lambda\epsilon_l\,\epsilon_x\,\epsilon_c\,\epsilon_d} , \tag{C4b}$$

where ϵ_p is evaluated by Eq. (C3b), λ is the excitation wavelength, h = Planck's constant, c = speed of light, and $\bar{n}$ is the average number of photons needed for dissociation. ϵ_l is the "wall-plug" laser efficiency for generation of CO_2 laser pulses of about 1–5 ns duration. For these short pulse durations, optimized overall optical design of megawatt-size CO_2 laser amplifiers involving multiple passes through the final amplifier stage should permit laser efficiencies approaching 5%.[50] Indeed, a CO_2 laser for large-scale deuterium separation will be nearly identical in many characteristics to the requirements for CO_2 laser fusion,[51] for which intensive development is well underway.[50,51] Extraction efficiences ϵ_x close to 100% are essential for process economics relating to redeuteration[45]; a (conservative)[45] value of 90%

is used here. The reaction chamber absorption efficiency ϵ_c is directly related to reaction chamber design optimization,[12] i.e., maximum multiple-pass optical path length consistent with desired beam energy fluence.[12] ϵ_c represents the percentage of light leaving the laser that is absorbed by an isotopic species; $1-\epsilon_c$ thus represents losses due to mirror absorption and light transmitted through the reaction chamber after many passes. Proper reaction chamber design maintains constant beam energy fluence, even though beam energy decreases due to absorption.[12] A reaction chamber efficiency of $\epsilon_c = 90\%$ will be used, which assumes multiple passes for a total optical path length of more than about 100 m.[12] Chamber designs with total optical path lengths of a kilometer have been considered for molecules with weaker absorption cross sections than the fluorocarbons being considered here.[12] The dissociation efficiency ϵ_d is defined as the product of the total number of dissociated deuterated molecules and the number of photons required to dissociate a single deuterated molecule (~ 30 for CDF_3) divided by the total number of photons absorbed by all deuterated molecules averaged over the beam cross section. In the wings of the beam, deuterated molecules absorb, but do not dissociate; consequently ϵ_d is strongly dependent on the beam intensity profile. ϵ_d is 1.0 for a rectangular beam profile at fluences above the saturation fluence. For the more realistic case of a Gaussian beam profile, ϵ_d is optimum at a peak fluence of about twice the saturation fluence,[52] for which ϵ_d has an optimum value of ~ 0.5,[52] the value to be used here.

Table VIII in the main body of the paper summarizes the estimated electrical energy required per separated deuteron for the separation stage of the three photochemical systems discussed in this paper. Also given in this table for comparison purposes are the total equivalent electrical energy requirements for conventional deuterium separation technology using the GS process.

The ~ 1% photon utilization efficiency of Freon 123 is an order of magnitude too low for practical utilization of this molecule. The 10% photon utilization efficiencies for either difluoromethane or trifluoromethane are good, and represent the only area of major potential process improvement. Significant improvement in photon utilization may be anticipated for trifluoromethane using two frequency dissociation. A first weak pulse with ~ 1 J/cm^2 fluence at 10.2–10.3 μ (resulting in absorption of 3–5 photons) simulataneous with a strong pulse at, say, 10.6 μ with 20–30 J/cm^2 fluence is expected to yield up to a threefold improvement in photon efficiency. This occurs for two reasons: First, the weak pulse experiences a higher deuterium optical selectivity of 2000–3000 precisely because it interacts with only the lower vibrational levels and, second, the strong pulse at 10.6 μ experiences two- to threefold weaker CHF_3 absorption compared to CHF_3 absorption at 10.2–10.3 μ (see Fig. 9). Since in the higher vibrational levels (in the quasicontinuum) the absorption features are shifted to relatively longer wavelengths than the corresponding ground state transitions,[53] excited CDF_3 should absorb at 10.6 μ. For difluoromethane a weak pulse at $P(8)$, 10.48 μ simultaneous with a strong pulse at 10.6 μ is expected to yield about a twofold improvement in photon utilization.

Makeup requirements

Since the deuterium dissociation selectivity is finite, a certain fraction of non-deuterium-bearing molecules is destroyed by each laser pulse. Equations (28) and (29) in the text give the amount of deuterated or protonated reagent $R_D(n)$ and $R_H(n)$, respectively, remaining after n pulses. The destroyed deuterium bearing molecules yield deuterium extracted with efficiency ϵ_x, and the ratio W of the total number of destroyed reagent molecules (working molecules) to extracted deuterium is thus

$$W=\frac{R_H(0)(1-e^{-\gamma_H n})+R_D(0)(1-e^{-\gamma_D n})}{\epsilon_x R_D(0)(1-e^{-\gamma_D n})} . \tag{C5}$$

For the experiments reported, $\gamma_H \ll \gamma_D < \sim 10^{-3}$ (see Tables IV–VI) and $n \le 50$; hence, $\gamma_D n \ll 1$ and Eq. (C5) may be rewritten as

$$W=\frac{R_H(0)\gamma_H+R_D(0)\gamma_D}{\epsilon_x \gamma_D R_D(0)} , \tag{C6}$$

$$=\frac{1}{\epsilon_x}\left(1+\frac{1-\delta}{\delta}\frac{\gamma_H}{\gamma_D}\right) , \tag{C7}$$

using Eq. (25). The ratio γ_D/γ_H is the intrinsic isotopic selectivity and is equal to or greater than the measured single-step deuterium enrichment factor β depending on the unknown (but apparently quite small) amounts of isotopic scrambling

$$\frac{\gamma_D}{\gamma_H} \ge \beta . \tag{C8}$$

Since the deuterium abundance δ is small ($\delta \ll 1$), Eq. (C7) may be rewritten using Eq. (C8):

$$W \le \frac{1}{\epsilon_x}\left(1+\frac{1}{\delta\beta}\right) . \tag{C9}$$

Recalling that W designates the number of destroyed working molecules per separated deuterium atom, Eq. (C9) is now used to write an expression for the amount of makeup working molecule per product D_2O. If M is the molecular weight of the working molecules, and since two separated deuterium-bearing molecules are required per produced D_2O molecule (molecular weight = 20), then the makeup requirement is given by

$$\text{makeup} \le \frac{M}{10\epsilon_x}\left(1+\frac{1}{\delta\beta}\right) . \tag{C10}$$

Expression (C10) is unitless, and is evaluated for all three working molecules and expressed in Table IX in the text as the number of kilograms of working molecule makeup required per kilogram of produced heavy water product. These replenishment costs should be economically assessed in light of present day costs. D_2O presently (1979) costs ~ \$300/kg (U.S.) and the halocarbon molecules cost ~ \$2–3/kg.[42] Only the makeup costs for CDF_3 and $CHDF_2$ are small compared to the GS D_2O production costs. Reimbursement for sale of end products such as C_2F_4 (in CDF_3) will somewhat lower makeup requirement costs.

Redeuteration of the working molecule

Redeuteration of the working molecules is essential to permit their reuse as is indicated in Fig. 21. The simplest way to achieve redeuteration is by isotopic chemical exchange with either water or natural gas (methane). Unfortunately, exchange is very slow without a catalyst for many molecules, and consequently the proper choice of catalyst and exchange medium is currently a necessary and quite active area of investigation.[21,45] In some cases isotopic exchange proceeds readily in water via the carbanion, catalyzed by added OH^- (base-catalyzed exchange). This occurs rapidly for Freon 123 according to the steps[17]

$$CF_3CHCl_2 + OH^- \xrightarrow{k_D} CF_3CCl_2^- + H_2O \ , \qquad (C11)$$

$$CF_3CCl_2^- + HDO \rightarrow CF_3CDCl_2 + OH^- \ , \qquad (C12)$$

for which the rate constants k_D are given in Table X in the text. Trifluoromethane isotopic exchange has been studied in methanol,[44] ammonia,[46] water/dimethylsulfoxide,[45(a)] and methanol/dimethylsulfoxide mixtures.[46] In these cases the catalyst is the sodium or potassium salt of the solvent, e.g., sodium methoxide (CH_3ONa) or potassium amide (KNH_2) for the first two listed possibilities.

If a nonaqueous solvent is used for exchange, then the solvent itself must first undergo redeuteration by isotopic exchange with water. Using ammonia as an example, the steps for the overall process may be written as

$$NH_3 + HDO \rightarrow NH_2D + H_2O \ , \qquad (C13)$$

$$CHF_3 + NH_2^- \xrightarrow{k_D} CF_3^- + NH_3 \ , \qquad (C14)$$

$$CF_3^- + NH_2D \rightarrow CDF_3 + NH_2^- \ . \qquad (C15)$$

Formation of the carbanion [step (C14)] is the rate-limiting step and its rate constant k_D is given in Table X. Step (C15) is very fast, since the carbanion is very reactive. The recycle of the solvent [step (C13)] would occur in an exchange tower separate from the isotopic exchange of the working molecule [steps (C14) and (C15)]. Both methanol and ammonia undergo rapid deuterium isotopic exchange with water without catalyst, Dimethylsulfoxide (CH_3SOCH_3) undergoes base-catalyzed exchange in water at a (relatively slow) second-order rate of 4.1×10^{-5} $1\,mol^{-1} \times s^{-1}$ at 69.5 °C (Ref. 48). For base-catalyzed exchange, the pseudo-first-order exchange rate K_{obs} is proportional to the catalyst anion concentration according to

$$K_{obs} = [RO^{-1}]\, k_D \ , \qquad (C16)$$

where $[RO^-]$ is the catalyst anion concentration in mol/l and k_D is the second-order rate constant given in Table X.

Table X summarizes the data available from the literature on liquid-phase deuterium isotopic exchange of the three working molecules under consideration. This table suggests that water is quite satisfactory for Freon 123 H/D exchange, but that use of a secondary solvent may be preferable for trifluoromethane, such as ammonia, or DMSO (dimethylsulfoxide). An extremely important consideration is the rate at which hydrolysis or solvolysis (in nonaqueous solutions) occurs, i.e., the rate at which the working molecule and catalyst are destroyed by irreversible reaction. This second-order rate constant k_{hyd} is given in Table X, where known. Ideally, a ratio $k_D/k_{hyd} > 10^4$ is desired to avoid excessive makeup requirements by hydrolysis. The ratio k_D/k_{hyd} is about 10^7 for Freon 123, indicating an ideal system with virtually no hydrolysis problems. For trifluoromethane, the data point at 70 °C in Table X indicates that hydrolysis will not be a problem for H/D exchange directly with water since the k_D/k_{hyd} ratio is $\sim 10^4$.[45(a)] This ratio is not known for trifluoromethane isotopic exchange in nonaqueous solvents, but may be even better than in water. However, the known solvolysis reaction between CHF_3 and ammonia[47] possibly renders ammonia less attractive. The very much faster deuterium exchange rates observed when dimethylsulfoxide is added to basic water[45(a)] (see Table X) make this an extremely attractive solvent system to consider. Thus, a H_2O/DMSO mixture catalyzed by NaOH is presently the best solvent system for achieving trifluoromethane isotopic exchange.[45(a)] Very little data exists in the literature on liquid-phase deuterium isotopic exchange of difluoromethane, although its base-catalyzed isotopic exchange is expected to occur significantly more slowly than for trifluoromethane, if it occurs at all. Slow homogeneous exchange catalyzed by Pt^{++} ion in solution has been measured[43] and is given in Table X.

The questions regarding adequate H/D exchange medium, exchange rate, and solvolysis rate remain to be more thoroughly investigated before large-scale photochemical deuterium separation can be implemented.

[1] E. S. Yeung and C. B. Moore, Appl. Phys. Lett. 21, 109 (1972).

[2] J. B. Marling, Chem. Phys. Lett. 34, 84 (1975).

[3] J. Marling, J. Chem. Phys. 66, 4200 (1976).

[4] L. Mannik, G. M. Keyser, and K. B. Woodall, Chem. Phys. Lett. 65, 231 (1979); 250-fold enrichment was reported therein, and 1650-fold enrichment was achieved at the same wavelength with improved UV lasers [K. Woodall (private communication)].

[5] V. S. Letokhov and C. B. Moore, Sov. J. Quantum Electron. 6, 129 (1976); 6, 259 (1976).

[6] J. C. Vanderleeden, Laser Focus 13(6), 51 (1977).

[7] G. Koren, U. P. Oppenheim, D. Tal, M. Okon, and R. Weil, Appl. Phys. Lett. 29, 40 (1976).

[8] J. B. Marling and I. P. Herman, Appl. Phys. Lett. 34, 439 (1979).

[9] I. P. Herman and J. B. Marling, Chem. Phys. Lett. 64, 75 (1979).

[10] I. P. Herman and J. B. Marling, J. Chem. Phys. 72, 516 (1980).

[11] S. A. Tuccio and A. Hartford, Jr., Chem. Phys. Lett. 65, 234 (1979).

[12] (a) J. C. Vanderleeden, Appl. Opt. 17, 785 (1978); (b) J. C. Vanderleeden, J. Appl. Phys. (in press).

[13] H. K. Rae, *Separation of Hydrogen Isotopes*, ACS Symposium Series (American Chemical Society, Washington, D.C., 1978), Vol. 68, pp. 1–26.

[14] F. T. Aldridge, I. P. Herman, J. B. Marling, and L. L. Wood, University of California Lawrence Livermore Laboratory Report UCID-17736-77-4 (1978) (unpublished); UCID-17736-78-1 (1978) (unpublished); UCID-17736-78-4 (1979) (unpublished).

[15] (a) J. G. Black, E. Yablonovitch, N. Bloembergen, and S.

Mukamel, Phys. Rev. Lett. **38**, 1131 (1977); J. G. Black, P. Kolodner, M. J. Schultz, E. Yablonovitch, and N. Bloembergen, Phys. Rev. A **19**, 704 (1979); (b) G. Koren and U. P. Oppenheim, Opt. Commun. **26**, 449 (1978); D. S. King and J. C. Stephenson, Chem. Phys. Lett. **66**, 33 (1979).

[16] Samples of Freon 123 were kindly made available by J. S. Lann, Development Product Sales, E. J. DuPont de Nemours & Co., Wilmington, Del.

[17] J. Hine, R. Wiesboeck, and R. C. Ghiradelli, J. Am. Chem. Soc. **83**, 1219 (1961); **83**, 1222 (1961).

[18] A. L. Henne and T. Midgley, Jr., J. Am. Chem. Soc. **58**, 884 (1936).

[19] (a) J. G. Atkinson, D. W. Cillis, and R. S. Stuart, Can. J. Chem. **47**, 477 (1969); (b) J. Hine, R. B. Duke and E. F. Glod, J. Am. Chem. Soc. **91**, 2316 (1969).

[20] I. P. Herman and J. B. Marling (unpublished results).

[21] K. B. Woodall, Ontario Hydro Research Centre, Toronto, Canada (private communication). Throughout this paper a nominal value of $\delta = 150$ ppm for CDF_3/CHF_3 is used.

[22] M. V. C. Sekhar, G. E. Millward, and E. Tschuikow-Roux, Int. J. Chem. Kinet. **5**, 363 (1973).

[23] D. Krajnovich and Y. T. Lee (private communication).

[24] S. F. Politanskii and V. U. Shevchuk, Kinet. Catal. **9**, 411 (1968) [translated from Kinet. Katal. **9**, 496 (1968)]; K. P. Schug, H. Gg. Wagner, and F. Zabel, Ber. Bunsenges. Phys. Chem. **83**, 167 (1979).

[25] Based upon a 62.2 kcal/mol endoergicity of Reaction (16) from Ref. 24 and thermochemical data from S. W. Benson, *Thermochemical Kinetics*, *2nd Ed.* (Wiley, New York, 1976).

[26] J. M. Simmie, W. J. Quiring, and E. Tschuikow-Roux, J. Phys. Chem. **74**, 992 (1970).

[27] M. V. C. Sekhar and E. Tschuikow-Roux, J. Phys. Chem. **78**, 472 (1974); B. E. Holmes, D. W. Setser, and G. O. Pritchard, Int. J. Chem. Kinet. **8**, 215 (1976).

[28] P. Kolodner, H. Kwok, J. Black, and E. Yablonovitch, Opt. Lett. **4**, 38 (1979).

[29] J. R. Nielsen, C. Y. Liang, and D. C. Smith, J. Chem. Phys. **21**, 1060 (1953).

[30] S. L. Chin and G. Boisclair, Opt. Lett. **4**, 340 (1979).

[31] A. Ruoff, H. Burger, and S. Biedermann, Spectrochim. Acta Part A **27**, 1359 (1971).

[32] D. H. Rank, E. R. Shull, and E. L. Pace, J. Chem. Phys. **18**, 885 (1950).

[33] J. B. Marling and I. P. Herman (unpublished absorption spectra of pure CD_2F_2); I. Suzuki and T. Shimanouchi, J. Mol. Spectrosc. **46**, 130 (1973); M. Mizuno and S. Saeki, Spectrochim. Acta Part A **32**, 1077 (1976).

[34] I. P. Herman, Opt. Lett. **4**, 403 (1979).

[35] C. R. Quick, Jr. and C. Wittig, J. Chem. Phys. **69**, 4201 (1978); N. V. Chekalin, V. S. Letokhov, V. N. Lokhman, and A. N. Shibanov, Chem. Phys. **36**, 415 (1979); J. C. Stephenson, D. S. King, M. F. Goodman, and J. Stone, J. Chem. Phys. **70**, 4496 (1979); Ph. Avouris, M. M. T. Loy, and I. Y. Chan, Chem. Phys. Lett. **63**, 624 (1979); R. D. McAlpine, D. K. Evans, F. K. McClusky, E. B. Selkirk, and S. L. Chin, Chalk River Nuclear Laboratory Report AECL-6455 (January, 1979).

[36] J. Black and E. Yablonovitch (private communication).

[37] See Ref. 15(b); and M. Rossi, J. R. Barker, and D. M. Golden, Chem. Phys. Lett. **65**, 523 (1979).

[38] E. R. Grant, P. A. Schulz, Aa. S. Subdo, Y. R. Shen, and Y. T. Lee, Phys. Rev. Lett. **40**, 115 (1978).

[39] See, for example, H. S. Johnston, *Gas Phase Reaction Rate Theory* (Ronald, New York, 1966); R. D. Levine and R. B. Bernstein, *Molecular Reaction Dynamics* (Clarendon, Oxford, New York, 1974).

[40] D. C. Tardy and B. S. Rabinovitch, Chem. Rev. **77**, 369 (1977).

[41] J. B. Marling, I. P. Herman, and S. J. Thomas, IEEE J. Quantum Electron. **15**(9), 22D (1979).

[42] J. S. Lann, DuPont de Nemours & Co., Wilmington, Del (private communication). Almost all halocarbons in bulk quantities cost \$2–3/kg (U.S. \$, 1979).

[43] L. F. Repka and A. A. Shteinman, Kinet. Katal **15**, 805 (1974) [Kinet. Catal. **15**, 722 (1974)].

[44] S. Andreades, J. Am. Chem. Soc. **86**, 2003 (1964).

[45] (a) E. A. Symons and M. J. Clermont, Chalk River Nuclear Laboratories Report AECL-6846 (January 1980); (b) A. I. Miller, Chalk River Nuclear Laboratories, Chalk River, Ontario, Canada (private communication).

[46] N. N. Zatsepina, I. F. Tupitsyn, A. V. Kirova, and A. I. Belyashova, Reak. Sposobn. Org. Soedin. **8**, 787 (1971).

[47] J. Jander and H. Nagel, Z. Anorg. Allg. Chem. **315**, 91 (1962).

[48] J. Jullien, H. Stahl-Lariviere, and A. Trautmann, Bull. Soc. Chim. Fr., 2398 (1966).

[49] See, for example, A. C. Baldwin, J. R. Barker, D. M. Golden, R. Duperrex, and H. Van den Bergh, Chem. Phys. Lett. **62**, 178 (1979).

[50] H. W. Friedman, Avco Everett Research Laboratory, Everett, Mass. (private communication).

[51] R. B. Perkins, "Laser Fusion Program at Los Alamos," University of California Los Alamos Scientific Laboratory Report LASL-79-29 (1979).

[52] I. P. Herman (submitted for publication).

[53] R. V. Ambartzumian, N. P. Furzikov, Y. A. Gorokhov, V. S. Letokhov, G. N. Makarov, and A. A. Puretzky, Opt. Commun. **18**, 517 (1976).